OPTIMIZATION FOR ROTOR TRACK AND BALANCE

A Thesis

Presented to the Faculty of the Graduate School

of Cornell University

In Partial Fulfillment of the Requirements for the Degree of

Masters of Science

by

Tauhira Hoossainy

January 2013

ABSTRACT

This investigation examines optimization methods for minimizing undesired vibrations in a helicopter. An iterative weighting system for adjusting emphasis of different flight conditions is implemented as an extension of current weighting schemes and performance results are discussed. Next, a cascaded method of least squares optimization is applied to incorporate minimization of vibrations at higher harmonics. A real coded genetic algorithm to prescribe integer-valued rotor modifications is then executed. Optimization methods are simulated using a linear sensitivity model to demonstrate the effects of rotor adjustments, specifically modifications in pitch change rod, outboard tabs, and hub weights on the Sikorsky S-76C++ aircraft. Applying an iterative flight condition weighting scheme with integer-bounded rotor adjustments while extending the range of harmonic frequencies included in the analysis develops a robust prescription of rotor adjustments. By virtue of their integer-based properties, these prescribed adjustments are more realistic and eliminate previously occurring loss of accuracy in implementation.

BIOGRAPHICAL SKETCH

Tauhira Hoossainy is graduating in January 2013 with a MS in mechanical engineering from Cornell University. Prior to attending Cornell, she earned her BS in mechanical engineering with a minor in computer science from the Georgia Institute of Technology. Her current research centers on developing heuristically optimized algorithms for helicopter rotor track and balance vibration minimization. She has also participated in research on human-robot sensor fusion and the development of an anticipatory controller using probabilistic graphical modeling. Through five internships at Lockheed Martin and General Motors, Tauhira has developed strong industrial leadership experience with roles from product design and development to manufacturing engineering. While at GM, she designed and implemented several autonomous robotic cells for various manufacturing assemblies. She has also led global research initiatives at the General Motors Proving Grounds, including developing and conducting experiments, then publishing results of accelerated climate studies for several highly controversial methods of roof-sealer production that directly affected processes in five plants across three countries.

In addition to her industry experiences, Tauhira has taught as a Teaching Assistant both at Georgia Tech and Cornell. She has served as the Head Teaching Assistant and the Course Manager for the only MATLAB course required for all Georgia Tech engineering students. She has also helped to teach undergraduate and graduate courses in the Mechanical and Aerospace Engineering department at Cornell and served as the Head Teaching Assistant for the Intro to Engineering summer course offered to Cornell pre-freshman.

To my family, whose unwavering support has always been a constant in my life.

ACKNOWLEDGEMENTS

This work was supported by funding from the National GEM Consortium and the Cornell College of Engineering. It would not have been possible without the support and expertise the Sikorsky Aircraft Corporation.

I would also like to give my deepest gratitude to the following people who have made this journey possible:

To Dr. Ephrahim Garcia for allowing me to pursue this opportunity to the extent of my capabilities and pushing me to be a better researcher and all-around person.

To Dr. Hod Lipson for believing in my potential and supporting me throughout my time at Cornell.

To Austin Fang, whose patient explanations helped to decode a technical world previously unknown to me.

To the members of the ASL and LIMS labs, Upson 127, and the MAE Administrative Staff who have been incredible colleagues and friends through their collaborations, guidance, and mentorship.

TABLE OF CONTENTS

LIST OF TABLES

LIST OF FIGURES

LIST OF SYMBOLS

n	multiple of the main rotor natural frequency, ex: $n \cdot$4.45 Hz, when representing multiple natural frequencies, n may be several numbers, ex: $n = 123$ represents the first through third natural frequencies
nP	S-76C++ main rotor n^{th} multiple of the natural frequency
$Z_n(k)$	vector of vibration velocities at modification step k for all sensors at the n^{th} multiple of the rotor natural frequency
T_n	airframe response matrix relating normalized RTB adjustments to $Z_n(k)$ data for the n^{th} multiple of the natural frequency
J_n	least squares regression scalar performance index for nP harmonics
θ_n	prescribed control adjustments based on the n^{th} multiple of the natural rotor frequency
W_{Zn}	weighting matrix for $Z_n(k)$ vibration data at the n^{th} natural frequency
W_θ	weighting matrix for impact of prescribed rotor adjustments
C_{123}	cost function minimized by integer-based real coded genetic algorithm
M	number of member solutions within a population
K	number of parents directly copied between generations through elitism
G	maximum generations for genetic algorithm
pC	probability of crossover for genetic algorithm
pM	probability of mutation for genetic algorithm
$ampScore$	scoring metric describing the sum of undesired vibration magnitudes
w^{amp}	flight regime weighting matrix used in calculating $ampScore$

CHAPTER 1

INTRODUCTION

Due largely to blade flexibility, uneven mass distribution, and irregularities in rotation, undesired vibrations are a frequent occurrence in helicopter operation. In addition to providing worker discomfort, system vibrations can cause premature damage to aircraft components and ultimately lead to accelerated failure [1,2,3]. The main rotor of a helicopter produces vertical vibrations through unequal lift from rotor blades and lateral vibrations from mass or vertical track imbalances. It is crucial to reduce both the vertical and lateral vibration levels within a helicopter in order to produce a nonhazardous and comfortable crew environment [4,5]. Rotor track and balance (RTB) is the method of prescribing modifications to the main rotor assembly of a helicopter in order to minimize undesired vibrations in the airframe to below an established threshold. Currently, RTB is performed primarily at the first harmonic frequency of the main rotor, which is understood to include vibrations having the highest effect on the human body [6,7,8,9,2].

Though the results of this study can be extended to other rotorcraft, the analysis described is tested on the Sikorsky S-76C++ helicopter, a 4-blade aircraft. RTB adjustments are typically based on measured vibration data using accelerometer vibration sensors integrated into a data acquisition system such as the General Electric Radar Acquisition Data System (RADS) [10,11]. Four physical sensors distributed throughout the cockpit of the aircraft and two vectorally-derived virtual sensors are used to measure vibration of the aircraft at each flying condition, known as a flight regime [12]. Vibration information from each sensor undergoes a Discrete

Fourier Transform to produce amplitudes and phases of undesired vibrations at every multiple from 1 to 12 of the main rotor's primary rotational frequency [13].

For the S-76C++, the 1/rev or $1P$ rotational frequency represents vibration amplitude and phase information at the natural frequency of the main rotor, which is approximately 4.45 Hz. The 2/rev, or $2P$ amplitude and phase represent vibration measurements for the aircraft at 8.9 Hz, and so forth. The flight regimes used for RTB data acquisition generally include ground, hover, and several forward flight airspeeds [2,14]. The five regimes at which vibration data is collected in this study are ground, hover, and forward flight at 125 knots (kts), 145 kts, and 155 kts.

The main rotor blades of the S-76C++ are typically referenced by color labels. When the tachometer and the magnetic sensor interrupter on the rotating swashplate of the main rotor mechanism are aligned, the black blade is at 0º relative to the forward centerline of the aircraft. In this configuration, the yellow blade is at 90º with respect to the forward pointing axis of the helicopter, the blue blade is at 180º, and the red blade is at 270º [6]. Possible adjustments on each blade of S-76C++ aircraft include an increase or decrease in the pitch control rod (PCR) of ± 30 notches, outboard tab adjustments in ± 40 thousandths of an inch from a horizontal baseline, and hub weights changes in the range of ± 80 ounces [12]. Adjustments to hub weights generally affect ground vibration of the aircraft system while lateral vibration is primarily affected by PCR adjustments, which are constant with speed, and tab adjustments, which become more impactful as the speed of the aircraft increases [1,15,16].

Due to the inherent symmetry of a four-blade rotorcraft, it has been shown that identical effects are produced from opposite adjustments of blades at a 180º offset [15,11]. Because of the

redundant effects of symmetrical adjustments, proposed PCR modifications can be reduced from ± 30 notch adjustments for each of the four blades in the S-76C++ to a change of ± 30 notches between each of the two blade pairs that are at a 180º offset from each other, as in black-blue and red-yellow. Similar adjustment reductions applied to tab and hub weight modifications make their possible solution spaces ± 40 thousandths of an inch and ± 80 ounces, respectively, for two pairs of blades per adjustment. Finding the product of each of the modification ranges per blade pair results in a solution space of 5.8982×10^{11} possible unique adjustment combinations. It is therefore not feasible to perform an exhaustive analysis of the solution space by evaluating every unique adjustment solution. However, computation can greatly be reduced with the application of a heuristic technique such as a genetic algorithm to more feasibly obtain a near-optimal solution.

Previous work has concentrated on minimizing the magnitude of undesired vibrations to below a threshold of 0.15 inches/second or ips at 1*P*. It is necessary, however, to explore minimization of higher frequency vibrations in order to produce a holistically improved vibration profile for the entire aircraft [2,6,8]. Traditional RTB tuning methods reduce unwanted vibrations via least squares regression models, neural networks, and other continuous numerical solving techniques [17,12]. These methods optimize the system for the best prescribed adjustments to the main rotor with results produced as continuous variables. However, in order to implement actual realistic adjustment solutions, these results must be rounded to integer values [18]. Data adjustment due to rounding causes decreased performance towards vibration minimization. Most modern RTB techniques are ill-equipped to handle optimization limited to integer-based solutions [10,19].

This study implements two novel methods for minimization of undesired vibrations within the airframe of the S-76C++ aircraft. An iterative method is first used to determine weighting factors for each flight regime of the helicopter, which are important parameters within the optimization scheme. This first optimization method involves extending the relationship between adjustments and vibration minimization into higher-order vibration frequencies from 1*P* to 3*P*, an important trend in RTB research [17,20,21]. The second method of optimization is an integer-based real valued genetic algorithm to heuristically minimize undesired vibrations at each of the first three natural frequencies. Blade modifications are presented as changes in PCR notches, outboard tab adjustments, and hub weights. The effectiveness of the proposed methods are evaluated through simulated implementation in 48 flights via a linear sensitivity model derived from experimental vibration measurements for the Sikorsky S-76C++ aircraft [6,17].

CHAPTER 2

LEAST SQUARES REGRESSION MODEL

2.1 Defining the Least Squares Regression Cost Function

The performance criterion used as the basis for both the cascaded minimization method and the genetic algorithm is found using Davis' minimum variance control algorithm at each harmonic frequency. This method relies on the linear model describing the effect of adjustments on a given set of measurements. A vibration measurement vector encompassing the magnitude and phase of the undesired vibrations for each of the 6 sensors and at all 5 flight regimes at adjustment step $(k+1)$ for the nP harmonics $Z_n(k+1)$ can be derived from the nP vibration measurements for the previous adjustment-step $Z_n(k)$ combined with the product of the experimentally-derived nP airframe response matrix T_n and the matrix of adjustment values θ_n for the PCR, outboard tabs, and hub weights, as represented in Equation 1 [6,11].

$$Z_n(k+1) = Z_n(k) + T_n \cdot \theta_n \tag{1}$$

The combination of the weighted squares of vibration measurements and applied controls for a particular nP harmonic is defined as the scalar performance index J_n in Equation 2 where W_{Zn} is a weighting matrix for the nP vibration data and allows for the emphasis or reduction in significance of vibration measurement values at each flight regime. The control weighting matrix W_θ allows for an increased influence, through penalty, to be placed on the PCR adjustments, outboard tab adjustments, or hub weight adjustments as desired based on operator constraints. In the case of this study, however, controller penalties are set to a constant matrix of zeros as exploring control weighting is beyond the scope of this analysis [11].

$$J_n = Z_n(k+1)^T \cdot W_{Zn} \cdot Z_n(k+1) + \theta_n^T \cdot W_\theta \cdot \theta_n \quad (2)$$

For the general least squares solution of a given set of vibration measurements at nP, a θ_n matrix of the adjustments necessary to minimize J_n can be found with Equation 3 which utilizes least squares regression by setting $\frac{\partial J_n}{\partial \theta_n} = 0$ and solving for θ_n. Proof of this least squares derivation can be found in Figure A1 in the Appendix [17].

$$\theta_n = -[T_n^T W_{Zn} T_n + W_\theta]^{-1} \cdot [T_n^T W_{Zn} Z_n(k)] \quad (3)$$

The matrix of applied controls found in Equation 3 represents the traditional method for obtaining the PCR notch adjustments, outboard tab modifications, and hub weight alterations necessary to optimize the rotor system in a way that minimizes vibrations at a specified rotor frequency of $n \cdot 4.45$ Hz [22,21,23,20]. In industry settings, this method is typically applied to the first harmonic frequency without addressing the influence of vibrations at higher frequencies.

The traditional least squares regression RTB method does not account for the importance of obtaining integer solutions. Optimal solutions are instead found in the continuous domain and rounded to the nearest whole number within adjustment constraints for implementation [17]. Since this method effectually seeks the best RTB modification profile and then deviates from this profile, the actual prescribed adjustments will sub-optimal. This can be demonstrated by Figure 1, which shows the effect of applying a rounded solution to the rotorcraft at each optimized harmonic.

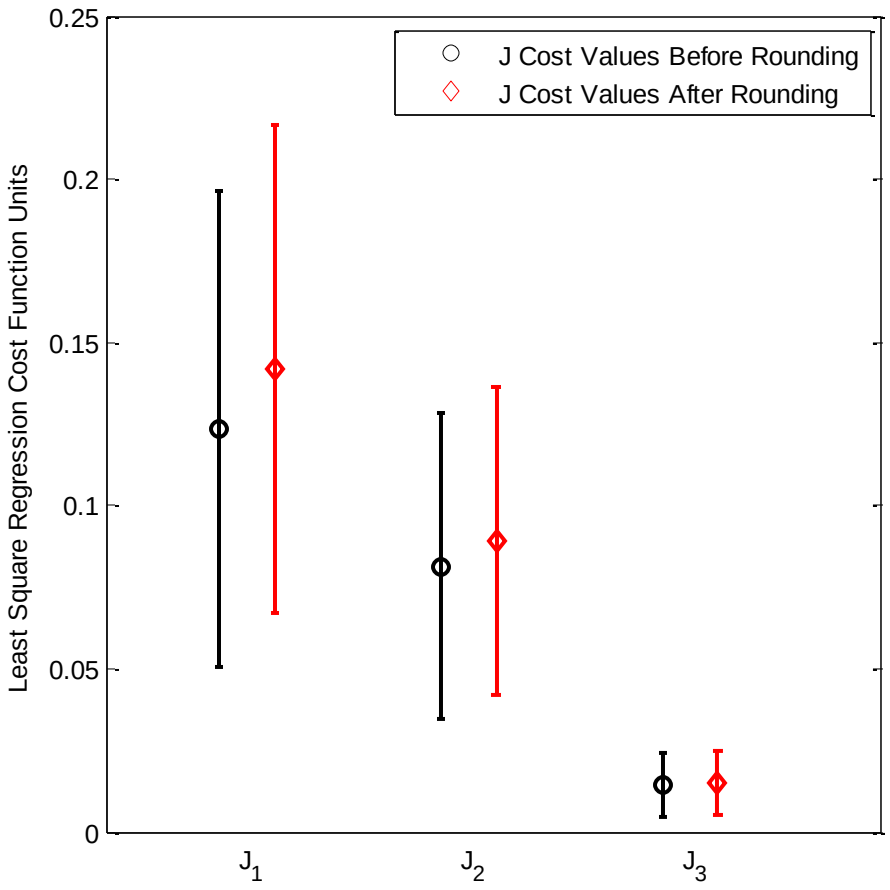

Figure 1. Least squares regression cost function values before and after rounding for a series of 48 flights at the first three harmonic levels

Rounding to integer values after performing the least squares regression optimization causes each of the minimized scalar performance index values to increase. While Figure 1 shows the effect of performance index trends from rounding, it is also noteworthy to examine the extent to which individual performance index values can vary due to rounding. Table 1 demonstrates the influence of rounding on the quality of the scalar performance index J_n of Equation 2 for each of the first three harmonics.

Table 1. Change in scalar performance index due to rounding for 48 flights

Scalar Performance Index	Average Change After Rounding	Standard Deviation of Change After Rounding
J_1	+ 17.56 %	± 14.30 %
J_2	+ 13.59 %	± 13.03 %
J_3	+ 4.71 %	± 3.13 %

As the goal of the least squares solution is to minimize the scalar performance index, the increase in performance index values at each harmonic frequency due to rounding demonstrates a decrease in performance when moving from the theoretical realm to practical system integration.

2.2 Iterative Development of Regime Weighting Parameters

As discussed in Equation 2, the least squares regression formula includes a weighting matrix W_{Zn} to represent different weighting values for each flight regime, or condition, over which vibration data is collected. For single or multiple harmonic analysis, it is possible to multiply W_{Z1}, W_{Z2}, and W_{Z3} with different weighting values to place varying degrees of emphasis on the $1P$, $2P$, and $3P$ harmonics respectively. However, the focus of this weighting investigation was not to vary weightings between different harmonic frequencies but instead to vary weightings across the different flight regimes. Emphasis is placed on determining regime weighting factors because the flight dynamics involved in ground and hover operation significantly differ from the flight dynamics at different forward airspeeds. Since most of the operation time for the aircraft is spent in forward flight, minimizing undesired vibrations in forward flight is a priority over reducing vibrations felt during the ground and hover regimes [3].

An iterative approach was taken to determine the best weighting scheme for each of the five flight regimes explored in this study. All of the weights were initially set to unity, making minimization across each flight regime equally important in the initial stages of the study. Vibration minimization was then performed over 48 sets of S-76C++ flight data using a least squares regression method applied to the first natural frequency data. The optimized solutions for each of the 48 sets of flight data were then implemented using the linear sensitivity model to determine the simulated aircraft behavior after applying each proposed balancing solution. Undesired vibrations with a magnitude of 0.3 ips or higher indicate significant rotor imbalance and a need for further rotor modifications to improve RTB [24,15]. Using this as a baseline, a count was taken across all six sensors and 48 flight sets for the number of times any of the flight regimes experienced vibration speeds above 0.3 ips.

For every instance where ground and hover have a vibration velocity at or above 0.3 ips after applying balancing techniques, the weighting values for ground and hover were respectively incremented by one unit. Since the regimes of forward flight are more dynamically complex and temporally significant, every instance over the 48 trials where a sensor detected undesired forward flight vibrations at or above 0.3 ips after balancing caused an increase of 3 to the weighting value of that particular forward flight regime. Adjusting the weighting modification value of forward flights by a multiple of 3 was found to add significant emphasis to the forward flying regimes while still allowing improved performance in the ground and hover regimes. The weights were then normalized by the maximum so that the highest regime weighting value was unity and the process was then restarted for a prescribed number of repetitions over the data set. This procedure allowed for emphasis to be placed on the flight

regimes most critical to the aircraft's mission or most disruptive to the overall stability of the vehicle.

CHAPTER 3

EXTENDING OPTIMIZATION TO HIGHER LEVEL HARMONICS

3.1 Cascaded Least Squares Regression

The cascaded harmonic method is a basic approach to extending the least squares regression vibration minimization to measurements at higher level harmonics. Recalling that $Z_n(k)$ represents vector of vibration amplitude and phase information for nP or the n^{th} multiple harmonics at adjustment step k, the initial measurement space encompassing $1P, 2P,$ and $3P$ is shown in Equation 4.

$$Z_1(k) \quad Z_2(k) \quad Z_3(k) \tag{4}$$

The adjustment profile found to minimize the measurements at the first multiple of the natural harmonic frequency is then found using the least squares regression method as outlined in Chapter Two. Equation 5 is a specific instance of Equation 3 that demonstrates the method to calculate θ_1, the series of adjustments necessary to minimize the system at $1P$. This equation utilizes the least squares regression model with the T_1 airframe response matrix, the W_{Z1} weighting matrix for first harmonic measurements, the first harmonic measurements represented by $Z_1(k)$ at the first adjustment step k, and the W_θ control impact weighting matrix.

$$\theta_1 = -[T_1^T W_{Z1} T_1 + W_\theta]^{-1} \cdot [T_1^T W_{Z1} Z_1(k)] \tag{5}$$

The adjustments found to minimize $1P$ are then applied to the measurements of Equation 4 with the airframe response matrix T_n for each harmonic to obtain updated measurement vectors for the new adjustment step $(k+1)$ based on the measurement vectors from the previous adjustment step. Calculating the updates for each of the first three frequency levels is an

extension of Equation 1 with the first harmonic level adjustments θ_1 found in Equation 4. Equations 6, 7, and 8 show the application of the adjustments for $1P$, $2P$, and $3P$, respectively.

$$Z_1(k+1) = Z_1(k) + T_1 \cdot \theta_1 \tag{6}$$

$$Z_2(k+1) = Z_2(k) + T_2 \cdot \theta_1 \tag{7}$$

$$Z_3(k+1) = Z_3(k) + T_3 \cdot \theta_1 \tag{8}$$

It is significant to note that to obtain the $Z_n(k+1)$ measurements at each harmonic level, the θ_1 adjustments based on the first harmonic were applied to the system at every harmonic level. Given these new measurements, the adjustment profile that minimizes the undesired $Z_2(k+1)$ vibrations, or the vibrations at the second multiple of the natural frequency, are then found. Equation 9 shows the formula required to find the θ_2 RTB inputs to minimize $2P$ vibrations based on the second harmonic airframe response matrix T_2, the second harmonic measurement weighting matrix W_{Z2}, and the control weighting matrix W_θ.

$$\theta_2 = -[T_2^T W_{Z2} T_2 + W_\theta]^{-1} \cdot [T_2^T W_{Z2} Z_2(k+1)] \tag{9}$$

In this instance, the second harmonic vibration measurements from adjustment step $(k+1)$ that already incorporate the θ_1 changes, $Z_2(k+1)$ are used instead of the original $Z_2(k)$ measurements.

The second harmonic adjustments θ_2 found from Equation 9 are then applied to obtain the updated $Z_n(k+2)$ measurements using the measurements from the previous adjustment step $Z_n(k+1)$ and the respective T_n airframe response matrices for each harmonic. Equations 10, 11, and 12 demonstrate the calculations for updating the measurements for the first three harmonic frequency levels.

$$Z_1(k+2) = Z_1(k+1) + T_1 \cdot \theta_2 \tag{10}$$

$$Z_2(k+2) = Z_2(k+1) + T_2 \cdot \theta_2 \tag{11}$$

$$Z_3(k+2) = Z_3(k+1) + T_3 \cdot \theta_2 \tag{12}$$

The measurements found for adjustment step $(k+2)$ only directly incorporate the θ_2 second harmonic adjustments because the $(k+1)$ measurements already integrate the θ_1 first harmonic adjustments. At this point in the analysis, the $(k+2)$ measurements have now been minimized for the first two multiples of the main rotor natural frequency. Given these updated measurements, the next step in the cascaded least squares regression optimization involves calculating the θ_3 adjustment prescription to minimize the $Z_3(k+2)$ measurements which have already been minimized for the first and second level harmonic frequencies. Equation 13 demonstrates the process of utilizing the $Z_3(k+2)$ measurements with the T_3 airframe response matrix and the W_θ and W_{Z3} adjustment and measurement weighting matrices to calculate the θ_3 alterations.

$$\theta_3 = -[T_3^T W_{Z3} T_3 + W_\theta]^{-1} \cdot [T_3^T W_{Z3} Z_3(k+2)] \tag{13}$$

The θ_3 RTB modifications can then be applied to obtain the measurements at the final adjustment step $(k+3)$ for each harmonic frequency level, as shown in Equations 14, 15, and 16. These equations again take advantage of the T_n airframe response matrices for each nP harmonic and the previous adjustment step measurement data, $Z_n(k+2)$ for each harmonic.

$$Z_1(k+3) = Z_1(k+2) + T_1 \cdot \theta_3 \tag{14}$$

$$Z_2(k+3) = Z_2(k+2) + T_2 \cdot \theta_3 \tag{15}$$

$$Z_3(k+3) = Z_3(k+2) + T_3 \cdot \theta_3 \tag{16}$$

Since the vibration measurements at $(k+2)$ incorporate first and second level harmonic adjustments, applying the θ_3 adjustments allows for a measurement profile which has been minimized for the first three harmonic frequencies in a sequential fashion. This cascaded least

squares regression method allows for optimization from $1P$ frequencies to $3P$ frequencies. Since the third harmonic level is the final harmonic level to be minimized, it can be expected that the measurements from this multiple of the natural frequency will demonstrate the most significantly improved performance. The cascaded method can also be approached by first minimizing the $3P$ harmonic level, then the second harmonic level and finally the first, or $1P$, harmonic level for results with a similar level of complexity.

The total adjustments applied with the cascaded linear regression model can be combined by Equation 17 to yield θ_{123}, a comprehensive set of adjustments.

$$\theta_{123} = \theta_1 + \theta_2 + \theta_3 \tag{17}$$

By uniting the θ_n tunings for each n-harmonic frequency multiple, the derived measurements at modification step $(k+3)$ based on the original measurements at modification step (k) are represented in Equations 18, 19, and 20 for the first, second, and third harmonic levels, respectively.

$$Z_1(k+3) = Z_1(k) + T_1 \cdot \theta_{123} \tag{18}$$

$$Z_2(k+3) = Z_2(k) + T_2 \cdot \theta_{123} \tag{19}$$

$$Z_3(k+3) = Z_3(k) + T_3 \cdot \theta_{123} \tag{20}$$

It can be mathematically proven that Equations 18 through 20 are equivalent to Equations 14 through 16 for obtaining measurements at the $(k+3)$ adjustment step since the θ_{123} total adjustment combines each of the individual harmonic adjustments. By utilizing Equation 18 through Equation 20, only one adjustment is necessary rather than three independent adjustments. After deriving this method, it is clear that the cascaded linear least squares

regression model allows for an extension of the analysis into a higher realm of multiples of the harmonic frequency.

3.2 Integer-based Real Coded Genetic Algorithm

Genetic algorithms are a subclass of evolutionary algorithms, which are heuristic methods inspired by the techniques of natural evolution to solve optimization problems. As an algorithmic analogy to evolution, genetic algorithms begin with a stochastically initialized population of M members where each member of the population is a possible solution [25]. While it is common to use strings of binary variables to represent population members within a genetic algorithm, it is also possible to perform optimization via a real coded genetic algorithm which formulates each population member as a series of real numbers [26].

When the solution space is continuous, as assumed in the basic and cascaded least squares regression methods previously described, it is sufficient to use a gradient-based optimization method. Because the physical rotor modifications are a range of discrete integer values, however, the optimization evolves into a combinatorial problem [27]. Instead of exhaustively calculating the combinatorial solution space, an integer-based real coded genetic algorithm can be used to minimize C_{123} the sum of the least squares cost functions for the first three harmonic frequencies.

$$C_{123} = J_1 + J_2 + J_3 \tag{21}$$

Weighting factors can also be applied to the cost function of Equation 21 to increase emphasis on various harmonic frequencies but this is not explored within the current study. In this case of RTB minimization, each member of the population is a 6-element set of adjustments for PCR notches, outboard tab modifications, and changes in hub weights between each pair of

blades following the previously outlined constraints for each type of adjustment and as shown in Figure 2.

PCR Δ black-blue	PCR Δ yellow-red	OB TAB Δ black-blue	OB TAB Δ yellow-red	HUB WT Δ black-blue	HUB WT Δ yellow-red

Figure 2. Solution layout for each population member of the genetic algorithm

At every step, or generation within the genetic algorithm, every member of the population is evaluated using the cost function of Equation 21. The primary operations for evolution within the genetic algorithm as applied to this problem are crossover, which is used to create the next generation from the current population, mutation, which uses a probability distribution to randomly perturb members of the new population, and elitism, which allows the best member or members of a specific generation to be copied over directly into the next generation.

There are several methods for selecting parents within a given population to produce the offspring that comprise the next generation. For the implementation of genetic algorithms used in this study, tournament selection is applied to determine pairs of parents when generating offspring. Tournament selection effectively mimics the competition aspect of natural mating. With each member of a given population having an equal probability of being chosen, two potential parents are selected at random and the parent with the lowest C_{123} cost (since in the RTB case it is desirable to minimize magnitude of vibrations) is chosen to be the first parent. The process of selection and competition is then repeated to designate a second parent.

Once two unique parents have been chosen, crossover within each type of modification (i.e. PCR, tab, and hub weight adjustments) is performed with a probability of pC. Throughout

this study, acceptance within a given probability is implemented by drawing random numbers from a uniform distribution on the open interval (0, 1) and comparing these numbers with the specified probability. If crossover occurs for PCR, for example, then the two children produced have one PCR modification value from each of the parents. If, however, crossover does not occur, one child will have the original two PCR modification values from one parent and the other child will have the two original PCR modification values from the other parent. The process of crossover occurs with equal probability of pC between all three sets of modifications, allowing for stochastically dynamic generation of two children that differ from the two parents where they originated.

The second element of genetic algorithms applied to this optimization is mutation, which occurs with a probability of pM, also determined from the parameter analysis. Once two children are produced via crossover, mutation is applied with a pM probability to each element of the new children. If an element of a solution is mutated, a random value is chosen from a uniform distribution within the constraints of the rotor modification represented by that element of the solution. For example, if a tab modification is to be mutated, a random integer between -40 and +40 is chosen to replace that particular tab value.

After crossover and mutation have been performed on the offspring of a generation, elitism is applied by directly copying the K best solutions from the current generation to the next generation. This elitism parameter K represents the number of 'fittest' population members that are maintained in future generations and allows the genetic algorithm to preserve the best solution or solutions already found without destroying them through crossover and mutation. The new generation is then comprised of the K best elements of the previous generation and the $M - K$ best solutions among the offspring produced. This process is repeated for a maximum

number of generations G, after which the best solution is reported. To ensure that this optimization method is robust to stochastics, several randomly-initialized trials must be run and results should be compared to ensure repeatability. Figure 3 shows pseudo code for the genetic algorithm heuristic as described by Sait and Youssef with modifications for current implementation [28].

```
Procedure (Genetic_Algorithm)
        M = Population size                 (* # of possible solutions at any instance *)
        G = Number of generations           (* # of iterations *)
        pC = Crossover probability          (* also called crossover rate Cr *)
        pM = Mutation probability           (* also called mutation rate Mr *)
        K = Elitism factor                  (* # of solutions carried directly to new population *)
        Ƥ ← Ξ (M)                           (* construct initial population Ƥ *)
                                            (* Ξ is the population constructor *)
        For j = 1 to M                      (* evaluate finesses of all individuals)
                Evaluate f(Ƥ[j])            (* evaluate fitness of Ƥ *)
        EndFor

        For i = 1 to Ng
                For j = 1 to No
                        (x,y) ← ϕ(Ƥ)        (* select two parents x & y from current
                                             population *)
                        offspring[j] ← Χ(x,y,pC)        (* with probability pC generate offspring by
                                                        crossover of parents x and y*)
                        mutated[j] ← μ(y)               (* with probability pM apply mutation *)
                Evaluate f(mutated[j])                  (* evaluate fitness of Ƥ *)
                EndFor
        Ƥ ← select (Ƥ,offspring)                        (* select best K solutions from parents and
                                                         best M – K solutions from offspring *)
        EndFor
        Return highest scoring configuration in Ƥ
End
```

Figure 3. Description of the genetic algorithm

CHAPTER 4

EVALUATION OF OPTIMIZATION TECHNIQUES

4.1 Results of Iteration for Regime Weighting Parameters

The iterative weighting scheme described in Chapter 3 was applied to 48 samples trials of flight data and was repeated over 25 iterations of each trial. Table 2 demonstrates that imbalances in the hover regime were easily dispelled to a manageable factor with no extra emphasis and that the two fastest forward airspeeds, 145 and 155 kts required the highest weighting factors to reduce unwanted vibrations.

Table 2. Regime weighting scheme after 25-iteration optimization over 48 trials

Flight Regime	Ground	Hover	125 kts	145 kts	155 kts
Weight	0.9549	0.0	0.6270	0.9810	1.0

Figure 4 shows polar plots of the two vectorally derived sensors, cockpit vertical and cockpit roll with vibration phase and amplitude information before and after adjustments for the first harmonics using an unweighted or unity weighting scheme versus using the weighting scheme of Table 2.

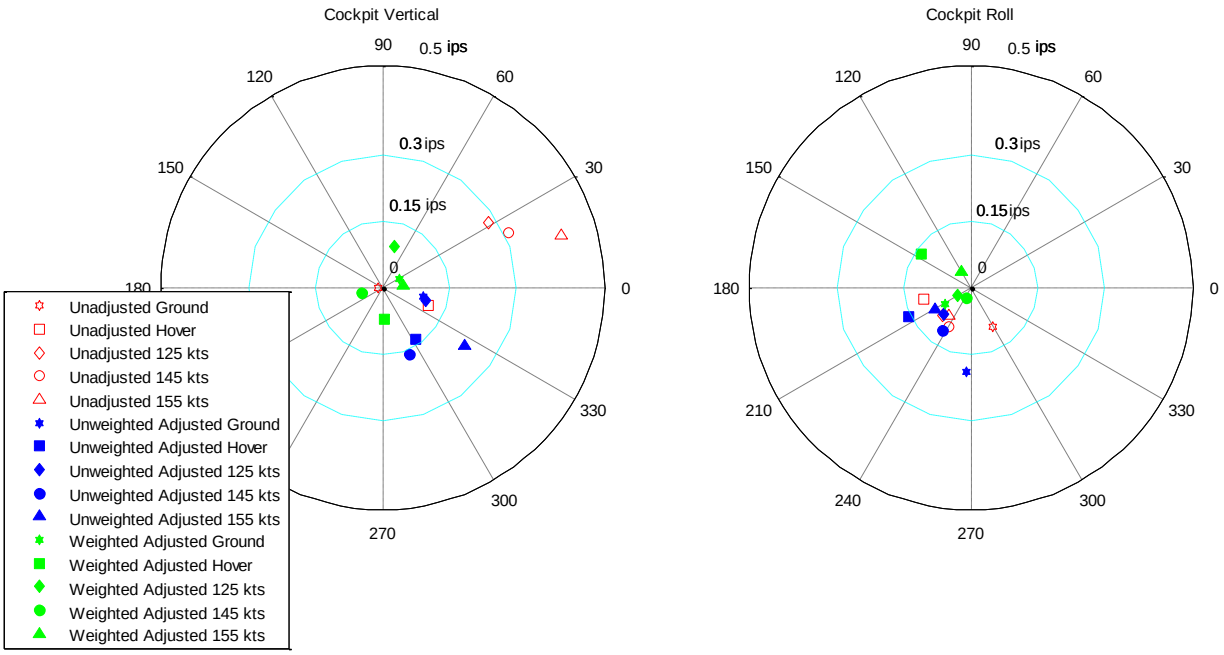

Figure 4. Polar plot of derived se nsor information before and after adjustment with: a) equal regime weightings and b) updated regime weightings

It is evident from Figure 4 that having a more complex regime weighting scheme allows for emphasis on the high-speed forward flight regimes while decreasing the importance of vibration minimization within hover, which is more easily reduced to within a tolerable range for this series of flight data. This iterative method of updating the weighting system allows for an improved overall performance between the different flight regimes and enables the weighted adjustments to all fall within the ideal 0.15 ips vibration range.

4.2 Establishing a Scoring Metric for Vibration Improvements

Both the cascaded harmonic method and integer-based real coded genetic algorithm optimization techniques were evaluated on 48 series of flight data for various S-76C++ aircraft. Based on each initial set of flight data, prescribed control adjustments were found and implemented in simulation through a linear sensitivity model. The effectiveness of each

approach to RTB minimization was quantified with a vibration amplitude score, or $ampScore$, describing the magnitude of the unwanted vibrations within each system. The amplitude scores of each modified system were then compared to the original unadjusted system, which serves as a baseline. In the formulation of $ampScore$, shown in Equation 22, r is varied from one to five to represent the five measurement regimes and s is varied from one to six to represent the six sensors used in vibration data collection (four physical and two derived sensors).

$$ampScore = \sqrt{\sum_{s=1}^{6}\sum_{r=1}^{5}\left(w_r^{amp} \cdot |amplitude\ of\ vibration|\right)^2} \tag{22}$$

The w vector referenced via r indices in Equation 22 is a vector of score weights which can be adjusted based on the relative importance of each regime for minimizing vibrations [3]. The w^{amp} vector used in this analysis is defined in Equation 23 and the weighting values are selected to focus twice as much scoring weight on the each of the forward flight domains as on the ground and hover regimes.

$$w^{amp} = \begin{bmatrix} 0.5 \\ 0.5 \\ 1 \\ 1 \\ 1 \end{bmatrix} \text{corresponding to} \begin{bmatrix} \text{ground} \\ \text{hover} \\ 125\ \text{kts} \\ 145\ \text{kts} \\ 155\ \text{kts} \end{bmatrix} \tag{23}$$

The $|amplitude\ of\ vibration|$ magnitudes are measured as positive distance directly to each vibration data point in ips from the origin, recalling that the origin represents 0 ips of vibration on a polar plot as shown in Figure 5.

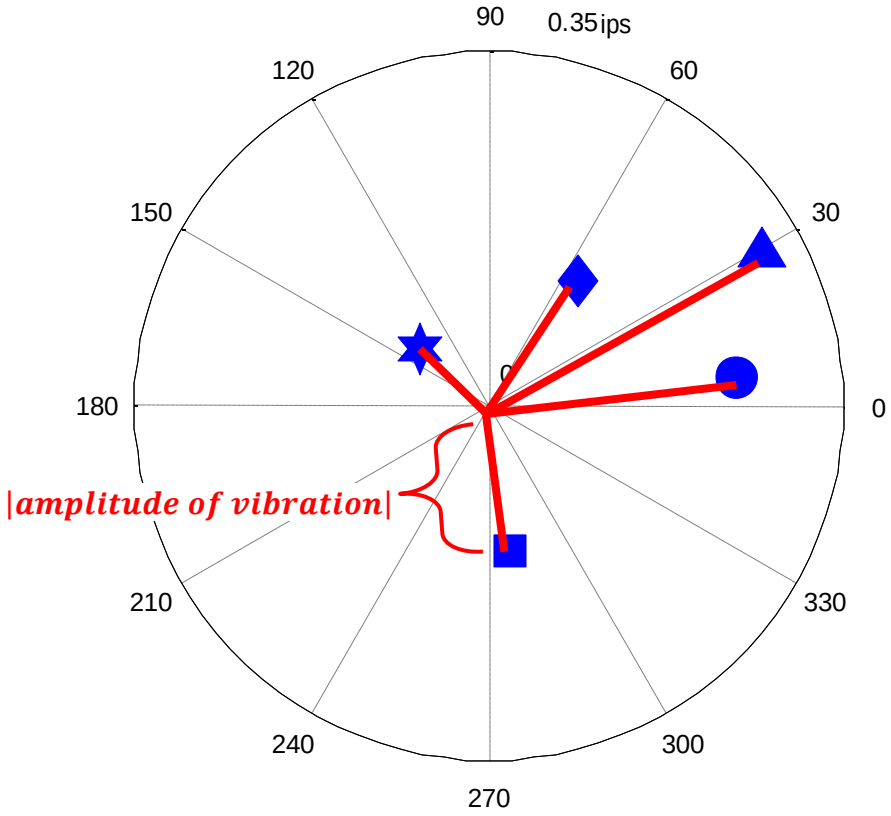

Figure 5. Polar plot demonstrating amplitude of vibration measurements

In order for an optimization method to perform better than the original unadjusted system, the $ampScore$ must decrease, which corresponds to a decrease in amplitude of unwanted vibrations. When comparing multiple optimization methods, it is desired that the change between the unoptimized system and the adjusted system result in a decrease in $ampScore$.

4.3 Least Square Regression Adjustments for First Harmonic Analysis

For every set of controller modifications found with each vibration minimization technique, polar plots were generated showing the changes in vibration magnitude and direction from the unadjusted system to the adjusted system simulated using the linear sensitivity model. Figure 6 shows the first harmonic vibration measurements before and after adjustment for an

instantiation of flight data at the first natural frequency. This flight data was adjusted using the least squares regression adjustments applied to the first harmonic of the main rotor. The rotor modifications to invoke the results in Figure 6 involve increasing the PCR at the black blade by two notches and the increasing the PCR by three notches at the yellow blade. The prescribed modifications also included adding nine ounces to the hub weights of the black blade and 35 ounces to the hub weight positioned on the red blade. Finally, this set of modifications incorporated a 0.009" increase in the outboard tab on the black blade and a 0.01" increase in the outboard tab on the red blade.

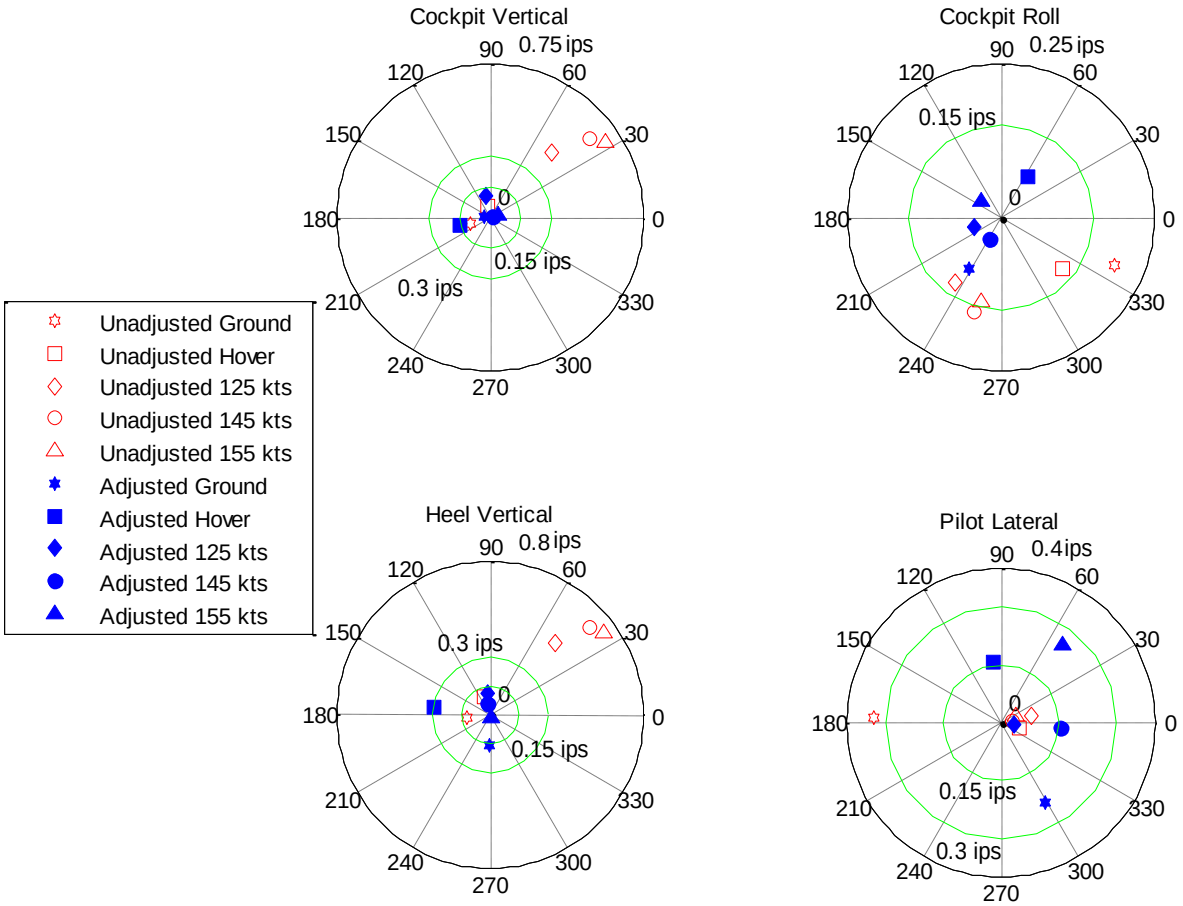

Figure 6. Polar plots of first harmonic sensor information before and after adjustment with adjustments optimized for only the first natural frequency

The four polar plots of Figure 6 represent the two vectorally-derived sensors and the two additional sensors which are not incorporated into the formulation of the derived sensors. In Figure 6, the system was optimized with the rudimentary least squares regression RTB method focusing on minimizing only the vibrations at the first natural frequency. The hollow red symbols represent vibrations in each flight regime before adjustments and the solid blue symbols represent vibration measurements after the optimal adjustments have been implemented. The larger green circles in cockpit vertical, heel vertical, and pilot lateral polar plots demonstrate the 0.3 ips threshold above which significant system imbalances are present. The smaller green circles in the cockpit vertical, heel vertical, and pilot lateral polar plots represent the ideal vibration minimization threshold of 0.15 inches per second. The cockpit roll polar plot of Figure 6 shows only the green threshold circle of 0.15 ips, as this polar plot is on a 0.25 scale since all vibration measurements from the cockpit roll derived sensor were under a magnitude of 0.25 inches per second. Figure 6 demonstrates that applying adjustments using the $1P$-focused least squares regression method minimizes vibration magnitudes at the cockpit vertical, cockpit roll, and heel vertical sensors. Based on the first harmonic sensor information in the pilot lateral polar plot for this flight instance, the adjustments to the aircraft only minimize vibrations in the ground flying regime, as the measurements in the other regime increase in magnitude after adjustment.

To further explore the efficacy of the $1P$-based adjustment method, it is necessary to see the effects of this adjustment method on higher level vibration data. Figure 7 demonstrates polar plots for the cockpit vertical, cockpit roll, heel vertical, and pilot lateral sensors for vibration at the second multiple of the harmonic frequency before and after adjustment for the same flight profile and adjustment conclusion of Figure 6.

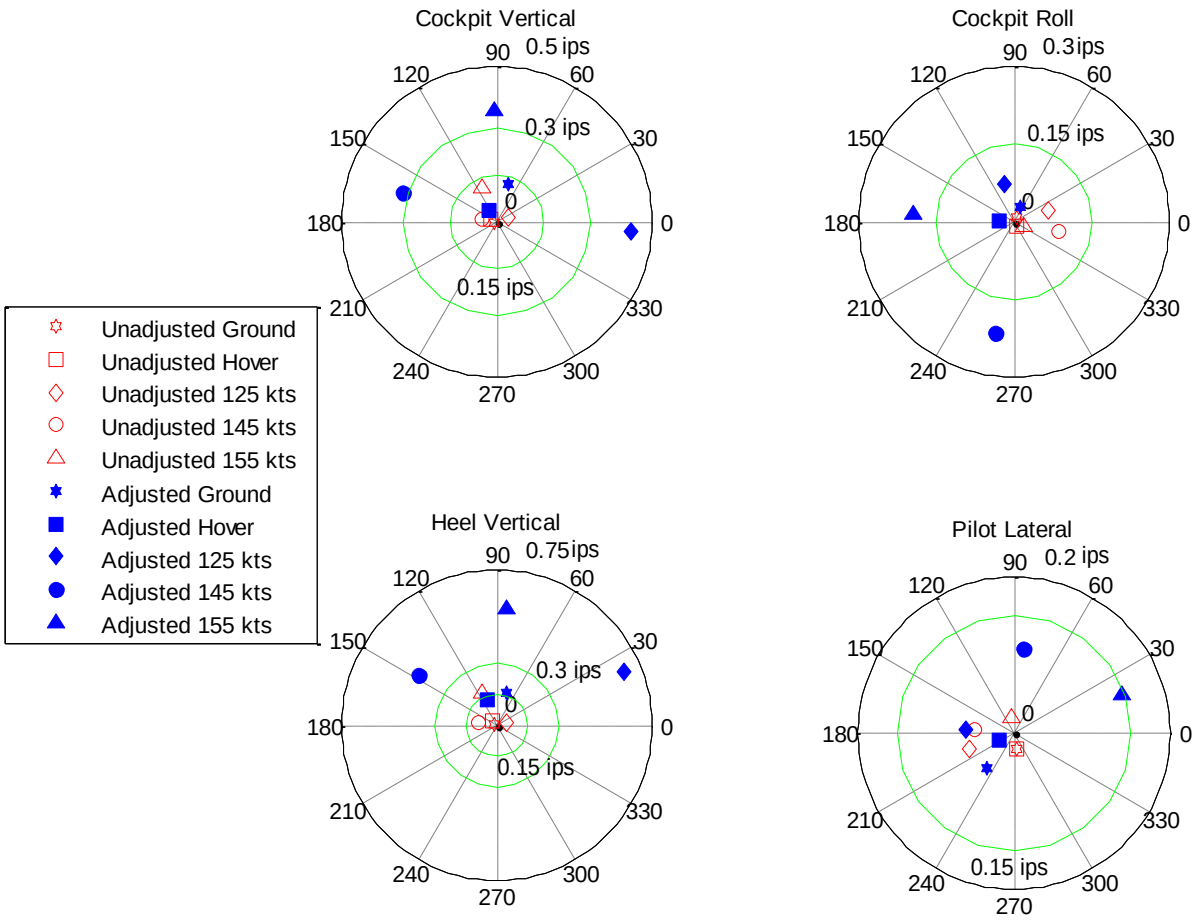

Figure 7. Polar plots of the second harmonic sensor information before and after adjustment with adjustments optimized for only the first natural frequency

From Figure 7, it can be seen that the general trends for the vibration magnitudes at the second harmonic frequency are to increase after adjustment. While the cockpit roll and pilot lateral vibration data is all of a magnitude less than the unbalanced 0.3 inches per second range, it is still problematic that these vibrations increase after implementing the RTB adjustments. For the cockpit vertical and heel vertical sensors, implementing the adjustments actually push all of the second harmonic vibration measurements for forward flight above the undesired 0.3 ips range. These undesired result are unsurprising because the first harmonic optimization least squares regression only minimizes vibrations for the first natural frequency of the system. Figure 8

illustrates the vibration sensor data before and after adjustments in the 3*P* harmonic realm for the same flight shown in Figure 6 and Figure 7.

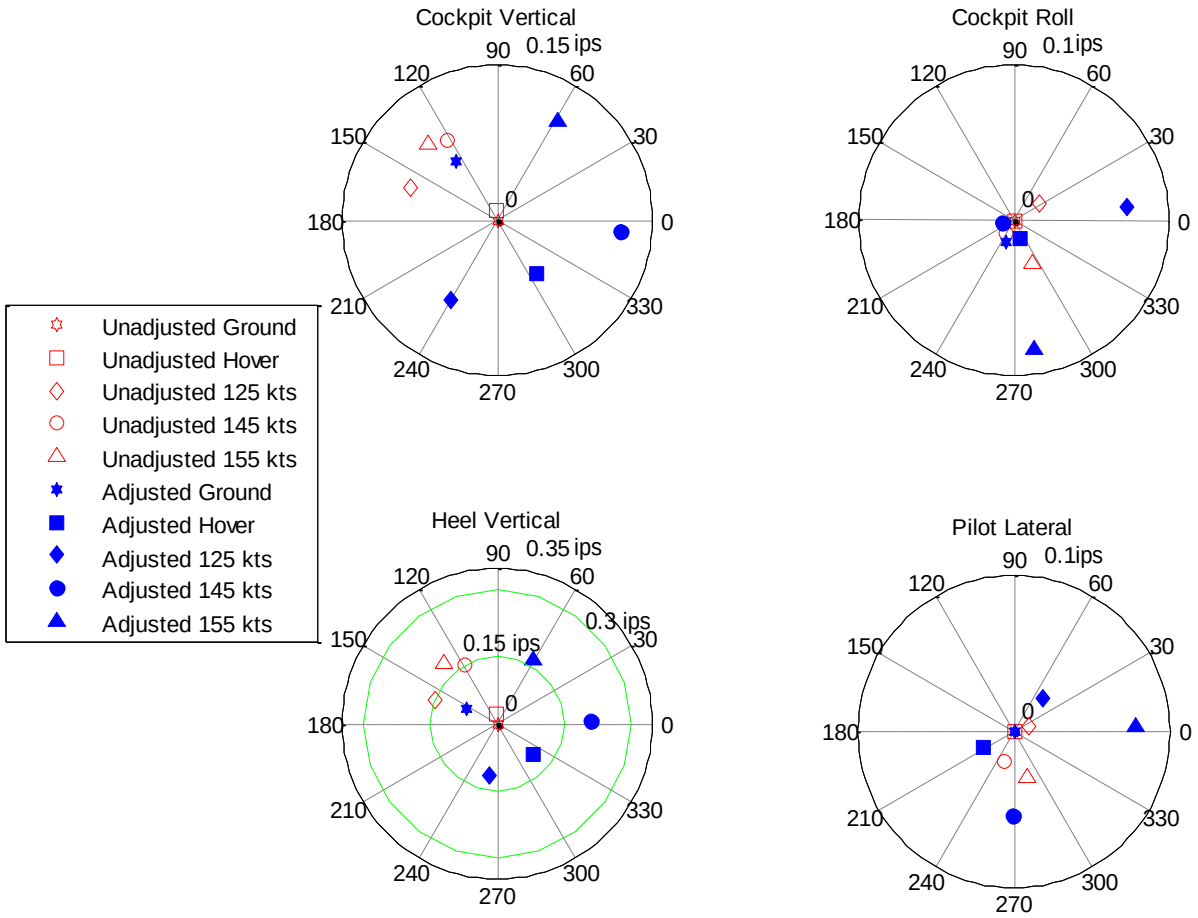

Figure 8. Polar plots of 3*P* vibration information before and after adjustment with adjustments optimized for only the first natural frequency

Since vibration magnitude increases after adjustments, the third harmonic vibration measurements follow similar trends as the second harmonic vibration information. In the 3*P* domain, the cockpit vertical, cockpit roll, and pilot lateral vibration profiles begin and remain smaller than the 0.15 inches per second threshold for this flight, however it is still less than ideal that the vibrations grow larger due to the RTB adjustments. For the heel vertical sensor, vibrations for the two fastest forward flight regimes, 145 kts and 155 kts, actually increase out of the optimal 0.15 ips range as a result of the prescribed modifications. Though at no point do

vibrations at the third multiple of the harmonic frequency reach the 0.3 inches per second range, the general increase in vibration amplitudes is not desired.

In this instance, the least squares regression model focused on the first harmonic frequency successfully reduces vibrations for the first natural frequency but does not have similar successes with higher frequencies. As previously discussed, the regime weighting scheme used to reduce vibrations for this optimization is described in Table 2. Table 3 shows the $ampScore$ values for each of the first three harmonic frequencies before and after adjustment via the $1P$ vibration least squares regression minimization method and using the scoring system described in Equations 22 and 23.

Table 3. Vibration amplitude scores after first harmonic optimization

	Unadjusted	Adjusted	Difference
$1P\ ampScore$	3.8447	0.8850	-2.9597
$2P\ ampScore$	0.6127	2.8474	2.2348
$3P\ ampScore$	0.7094	0.9276	0.2182

While the $ampScore$ value is reduced for the first natural frequency, the vibration at higher level harmonics is not reduced. It is evident from Table 3 and from Figure 6 through Figure 8 that this basic least squares regression performs significantly better for the first harmonic than for the second and third level harmonics.

4.4 Cascaded Least Square Regression Adjustment Prescription

As the RTB optimization methods are expanded to include higher level harmonics, a balance must be established between optimizing across the first three harmonic frequencies and minimizing vibrations purely for the first harmonic frequency of 4.45 Hz. Given the same flight

system from the previous analysis regarding the 1*P* least squares regression optimization, the adjustments found involve adjusting the black blade by incrementing the PCR two notches, increasing the outboard tab by 0.002", and adding 19 ounces to the hub weight. Additionally, the PCR is increased by two notches at the red blade and the hub weight of the red blade is increased by 14 ounces. Figure 9 shows the 1*P* vibration results before and after adjustments via the cascaded method of optimization.

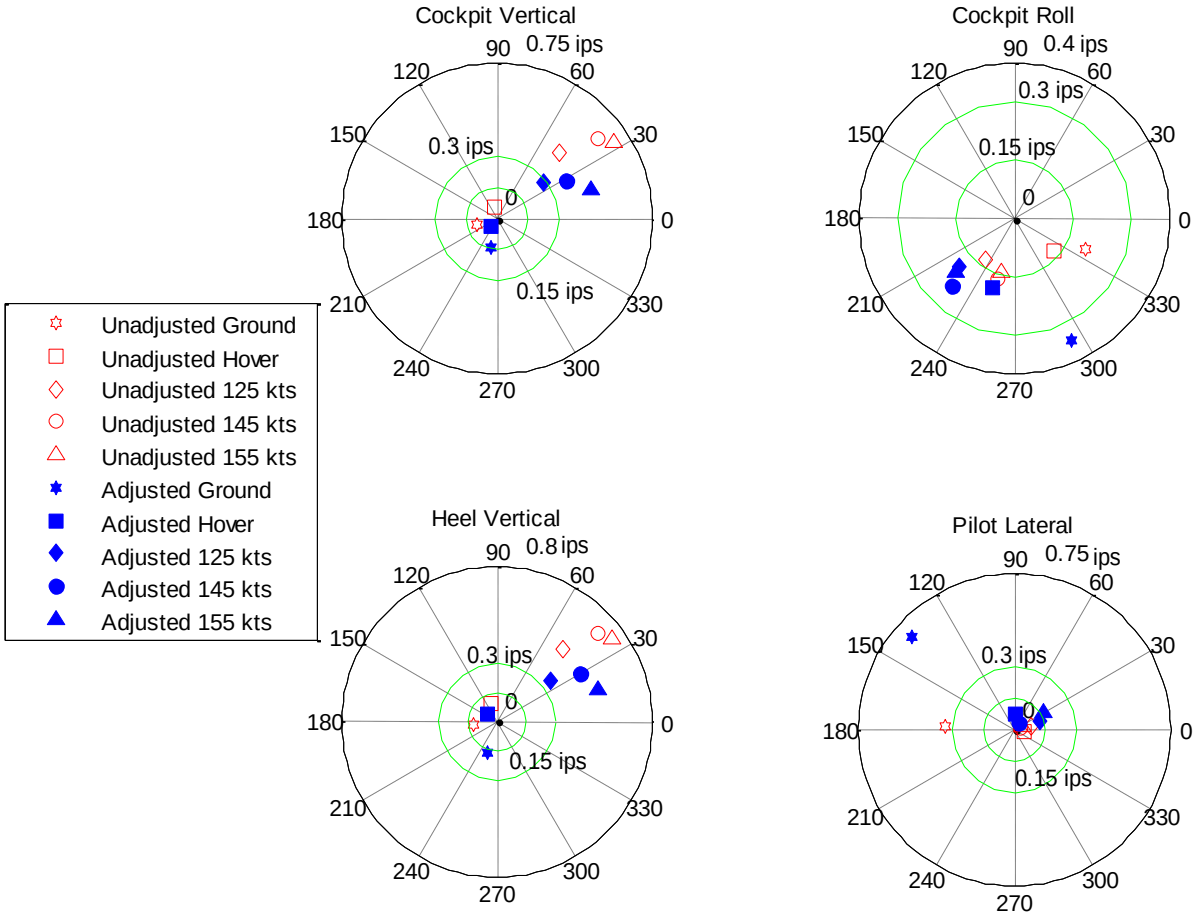

Figure 9. First harmonic frequency vibration information before and after adjustments found via cascaded optimization method

The amplitudes of vibration for the first harmonic frequency are primarily decreased in the cockpit vertical and heel vertical after applying the adjustments from the cascaded optimization method. The vibrations in the cockpit roll and pilot lateral sensors however, are

increased out of the desired 0.15 ips range but not to the extreme of the 0.3 ips range except in the case of the ground flight regime. Comparing 1*P* vibration performance due to the first harmonic-focused least squares regression method and the cascaded least squares regression method, it is clear that the first-harmonic focused least squares regression method is superior at minimizing first harmonic vibrations. This loss of first-harmonic efficacy for the cascaded method is expected since the first harmonic frequency is not the solitary focus of the cascaded optimization. Vibration in the realm of the second multiple of the rotor natural frequency before and after the cascaded adjustment is shown in Figure 10.

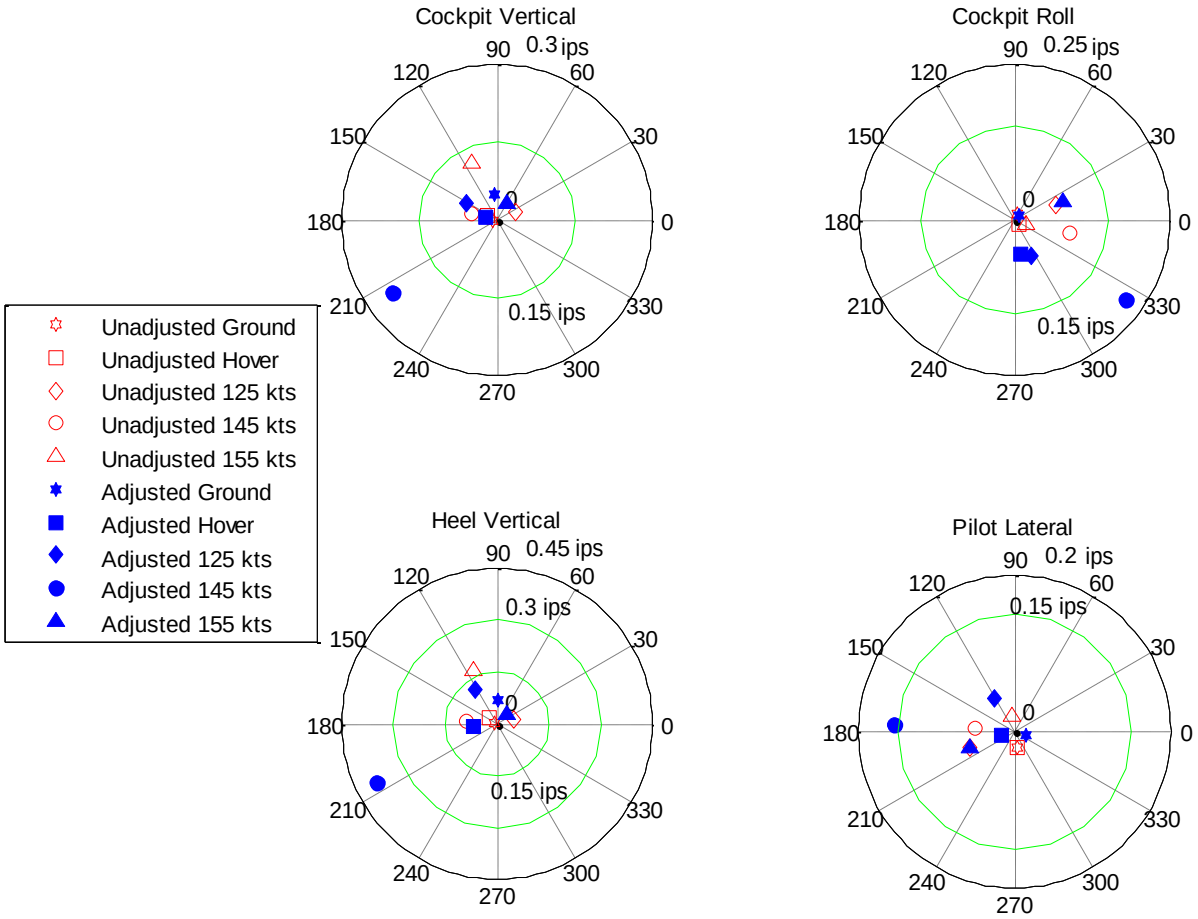

Figure 10. Second natural frequency vibration profile before and after cascaded optimization adjustments

The sensors shown in Figure 10 generally demonstrate a decrease in magnitude of vibration due to adjustments from the cascaded method. The most notable exception is within the realm of forward flight at airspeeds of 145 kts, which increases from cascaded adjustments in all sensors. Only in the heel vertical sensor do these vibrations accrue beyond the 0.3 ips threshold. The vibrations at the second harmonic frequency in the cockpit vertical, cockpit roll, and pilot lateral sensors all remain at or below the ideal 0.15 inches per second limit. This performance, while not impeccable, is far superior to the $1P$ least squares regression optimization at the second harmonic frequency.

As the cascaded optimization method incorporates first, second, and third multiple harmonics into the RTB minimization, it is important to examine Figure 11, which demonstrates $3P$ vibrations across the two derived sensors and two of the physical sensors of the flight system.

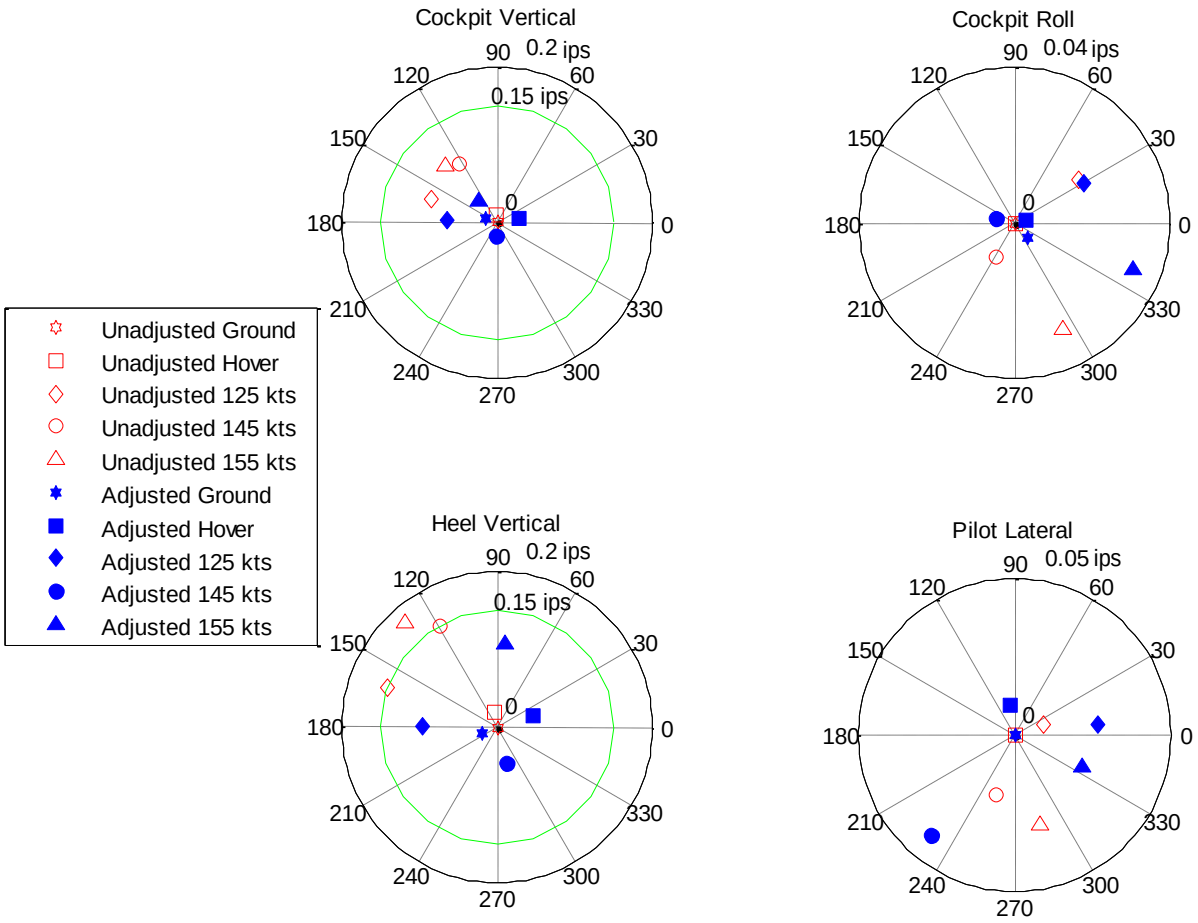

Figure 11. Changes in vibration at the third natural frequency from cascaded optimization

While vibration measurements in the heel vertical start above the 0.15 inches per second range, as evidenced by the green circle indicating that range, the cascaded method is able to reduce $3P$ vibrations in all regimes to a desired level. In the case of the cockpit roll and pilot lateral sensors, the vibrations across each flying regime either stay the same or increase due to adjustments. Though it would be preferable if the vibrations in the cockpit roll and pilot lateral sensors decreased from the RTB adjustments, these vibrations are well within the ideal 0.15 ips subspace. For this flight information, the cascaded method is superior to the $1P$ least squares regression method at minimizing $3P$ harmonic vibration in the cockpit vertical and heel vertical sensors.

The scoring metrics from Section 4.2 are instructive in showing changes due to the cascaded harmonic method of vibration reduction. Differences in $ampScore$ magnitudes before and after implementing adjustments for this aircraft are shown in Table 4.

Table 4. Changes in vibration amplitude profiles after cascaded harmonic optimization

	Unadjusted	Adjusted	Difference
$1P\ ampScore$	3.8447	2.9498	-0.8949
$2P\ ampScore$	0.6127	1.1411	0.5285
$3P\ ampScore$	0.7094	0.3958	-0.3136

Though the $1P$ least squares regression method creates a tighter vibration profile across the first level harmonics than the cascaded method, as seen by comparing Table 3 with Table 4, utilizing the modifications from the cascaded method produces lower scores for both first and third level harmonic frequencies. The previous least squares regression optimization, by comparison, only reduces the $ampScore$ for first level harmonics. While the $ampScore$ at $2P$ harmonic frequencies for both methods worsen due to implementing modifications, the change to the score is much less detrimental due to the cascaded method than from the original least squares regression method. The sensor polar plots and $ampScore$ values demonstrate that for this flight instance, the cascaded method does improve vibration performance at the second and third multiples of the natural frequency for the main rotor, as compared to the $1P$ least squares regression.

4.5 Rotor Modifications Found via Genetic Algorithm Optimization

Recall from Chapter Three that the parameters of importance for the genetic algorithm include the M number of member solutions within a population, the K number of parents directly

mimicked through elitism, and the G maximum number of generations evaluated within the scope of the algorithm. After exploring the RTB problem through empirical testing over a range of variables, it was found that the real coded integer-based genetic algorithm converges to a level of desired accuracy via a value of M = 100 solutions within a population evolving over $G = 80$ generations with $K = 1$ parent copied directly from one generation to the next via elitism.

Probability of crossover pC and probability of mutation pM are also essential elements to determining the fluidity of the genetic algorithm as it explores the solution subspace [25]. There are several methods, such as those suggested by Reed et. al., for genetic algorithm parameter selection based on asymptotic analysis of how the heuristic converges [29]. However, asymptotic analysis is based on the assumption that an arbitrarily large number of evaluations are feasible, which is not always the case when incorporating limitations of computation power, evaluation time, etc. For practical applications such as heuristic optimization for RTB, it is more appropriate to set genetic algorithm parameters via empirical tuning over trial runs of the genetic algorithm with a smaller population in a limited number of generations.

Parametric analysis was performed for probability of crossover pC and probability of mutation pM values ranging from 0.2 to 0.8 in steps of 0.05 for probability of crossover and probability of mutation with $K = 1$ and all other genetic algorithm parameters reduced by 50% (making population size M = 50 solutions evolve over $G = 40$ generations). Flight data was optimized for 12 test cases of the S-76C++ and averaged over 3 randomly initialized trials to ensure that the parameter selection method is robust to stochastics. From the 169 possible parameter combinations examined, permutations that included average and standard deviation $ampScore$ values in the smaller 33% for the first three harmonic frequencies were then isolated for further exploration and are shown in Figure 12.

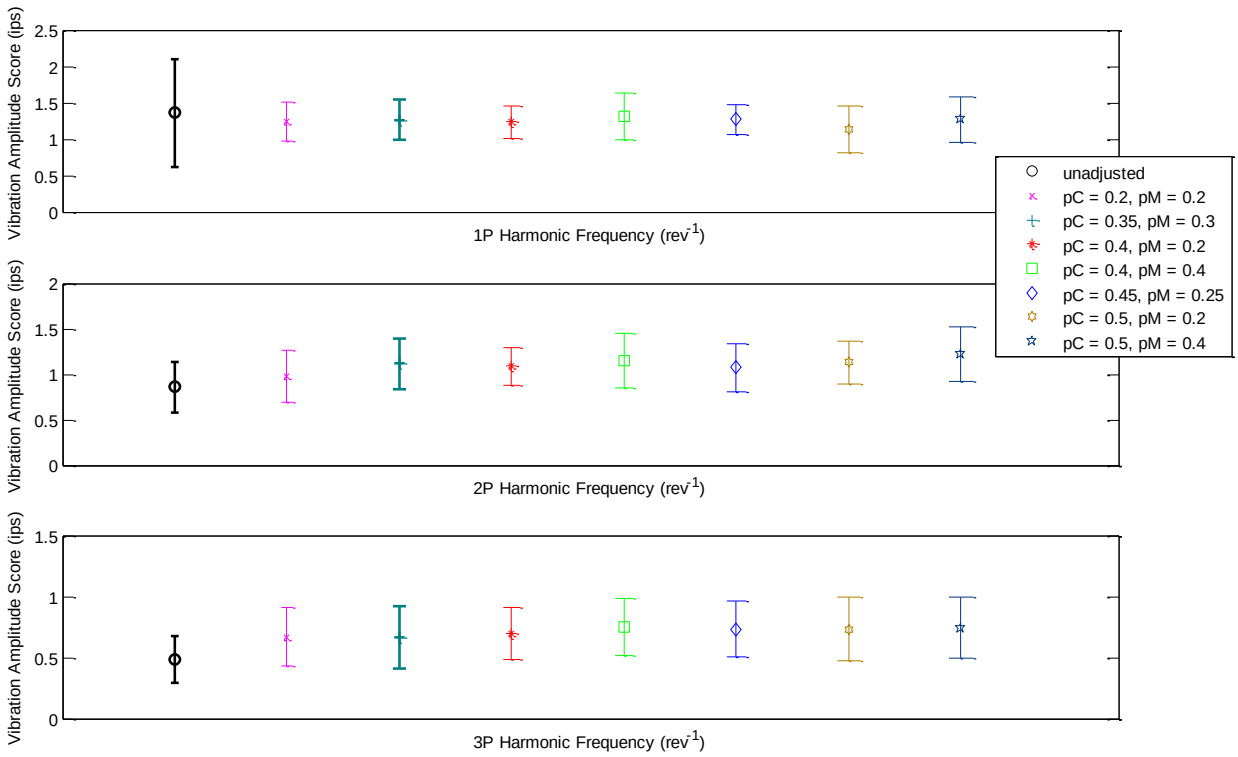

Figure 12. Scoring results of parametric analysis for pC and pM genetic algorithm factors

The final parameter combination chosen was $pC = 0.35$ and $pM = 0.3$ because it produced the lowest mean scores and standard deviations over all of the flight information tested.

After establishing the optimization parameters for the integer-based real coded genetic algorithm, this heuristic method was implemented across all 48 sets of S-76C++ flight data. As a result of the stochastic nature of genetic algorithms, including the randomized population initialization and the probabilistic nature of reproduction, it is necessary to ensure that the optimization performance is resilient to stochastics. As a result, each collection of flight data was optimized with 6 instantiations of the genetic algorithm. This allows a demonstration of the convergence of the algorithm even in the face of stochastic uncertainties, as shown in Figure 13.

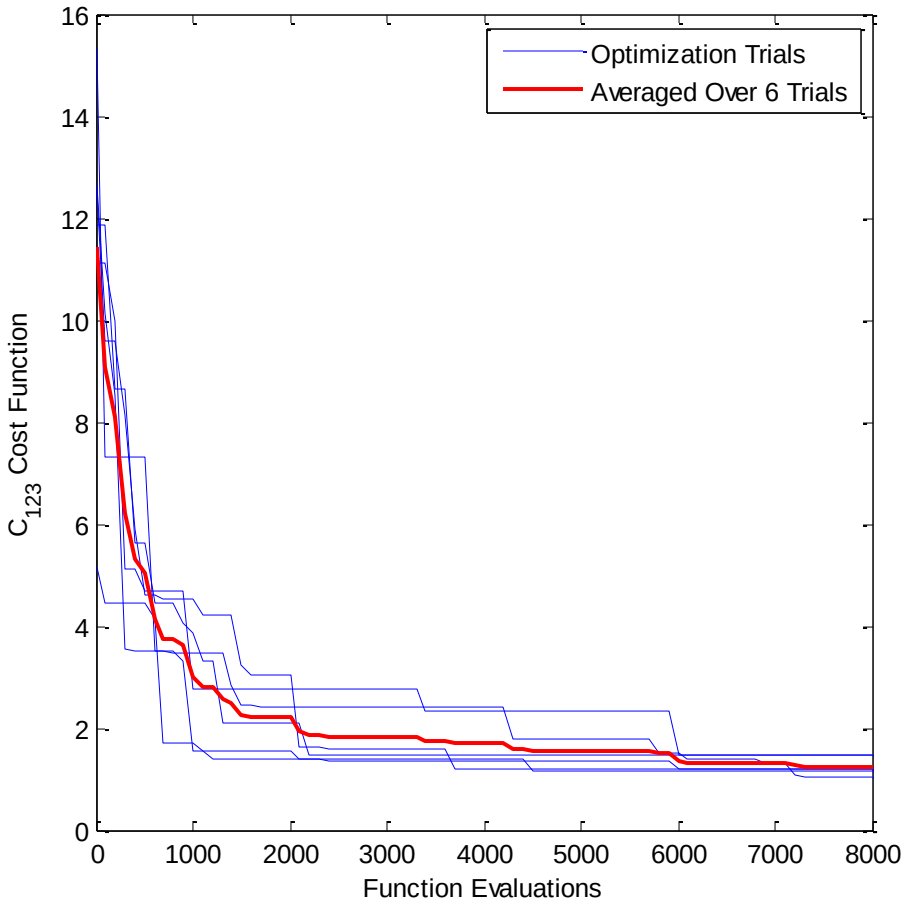

Figure 13. Convergence of C_{123} cost functions with respect to function evaluations

As can be seen in the figure, each instantiation of the genetic algorithm initiates with a very different cost function value but by approximately 6000 function evaluations, the cost function value of the best solution for each initialization has converged to within ± 12.1% of the average best cost functional solution. The adjustments found from each of the RTB minimizations using genetic algorithms were then applied with the linear sensitivity model as previously discussed. Figure 14 displays first harmonic vibration magnitude and phase information for the same instantiation of flight data as shown with the previous optimization methods.

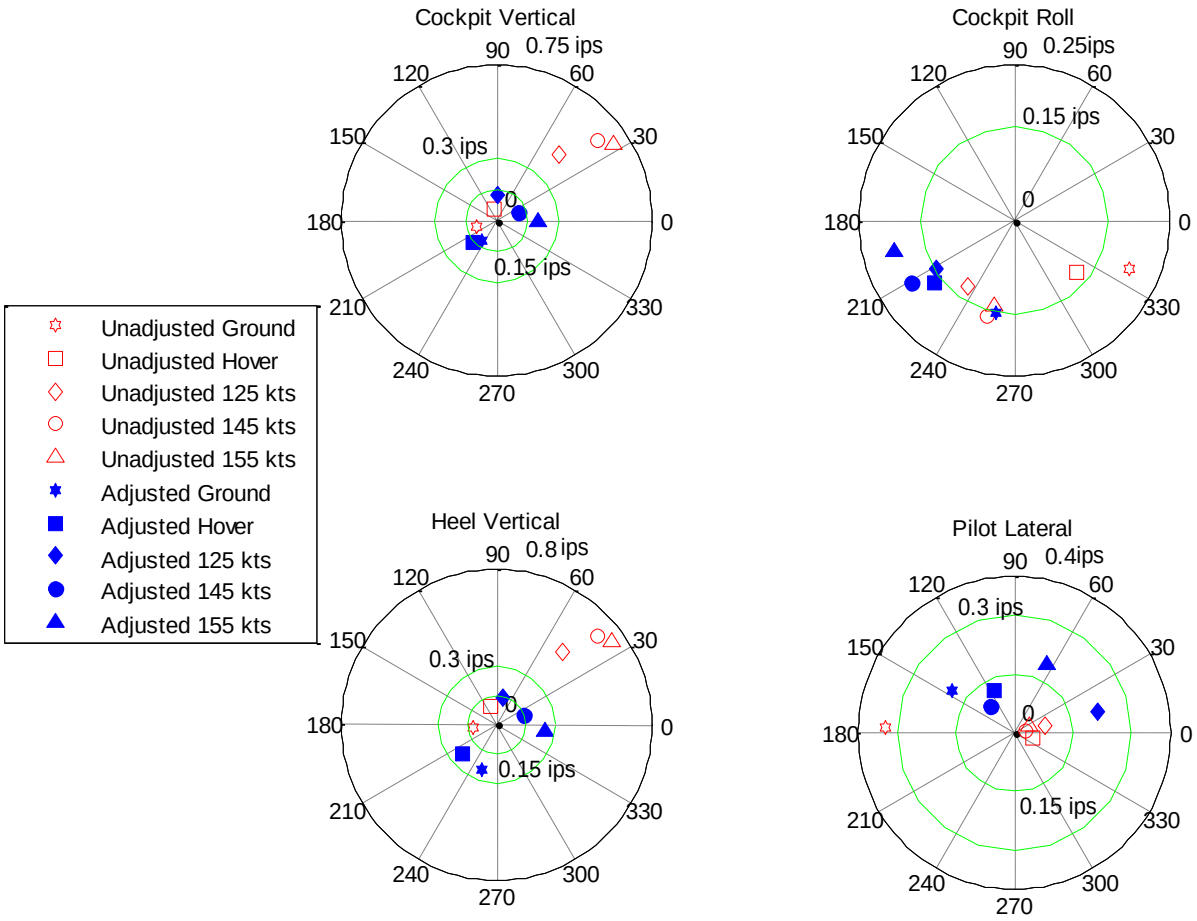

Figure 14. First harmonic vibration results via RTB by genetic algorithm optimization

This vibration information at the first harmonic frequency is shown across the cockpit vertical, cockpit roll, heel vertical, and pilot lateral sensors. The prescribed adjustments involve a three notch increase in the PCR at the black blade and a three notch increase in the PCR at the red blade. Additionally, the black outboard tab is increased by 0.007", the yellow outboard tab is increased by 0.001", the hub weights of the blue blade are increased by 3 ounces and the hub weights of the red blade are increased by 15 ounces. These RTB changes allow for the vibration amplitudes at every regime across all four sensors to be established under the 0.3 ips unbalanced point. However, although the vibration measurements are all under the undesired limit, the first harmonic pilot lateral vibration measurements are increased and the cockpit roll vibration

amplitudes retain approximately the same magnitude due to the implemented rotor modifications. While comparing Figure 14 with Figure 6 demonstrates that the $1P$ least squares regression method performs better at minimizing cockpit roll sensor vibrations than the genetic algorithm approach, performance at each of the other sensors is comparable for the first harmonic. The heuristic optimization approach to RTB is also better at minimizing cockpit vertical, cockpit roll, and heel vertical flight information at the first natural frequency than the cascaded harmonic method. The $1P$ vibration data from the cascaded harmonic method, as shown in Figure 8, is comparable in its effects on the pilot lateral sensor information, except in the ground regime, where the heuristic optimization produces superior minimization.

Similar to the cascaded method, the real valued genetic algorithm approach to RTB also incorporates higher frequency profiles. The vibration data of the second rotor frequency is displayed before and after heuristic optimization adjustment in Figure 15.

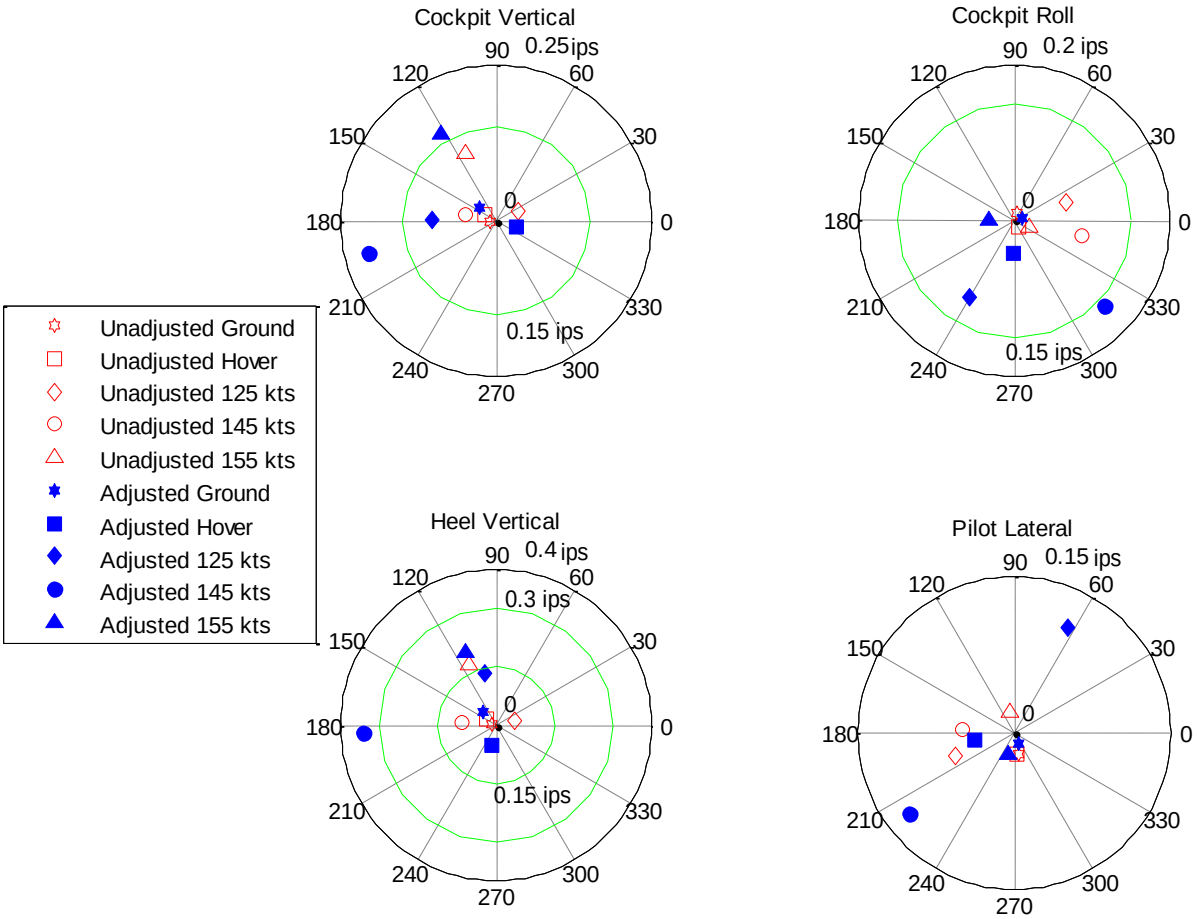

Figure 15. Vibration profile before and after heuristically optimized RTB adjustments

For the second harmonic frequency, forward flight at 145 kts produces the most vibrations across each sensor. These forward flight vibrations only exceed the 0.3 inches per second unbalanced standard in the heel vertical sensor. Regardless, the heuristic optimization RTB method does not produce significantly minimized second natural frequency vibrations. While this second harmonic level provided challenges for each optimization method explored with this instantiation of flight data, heuristic optimization performed slightly better than the cascaded method at minimizing secondary harmonic vibrations. The genetic algorithm method also performed substantially better at minimizing undesired secondary harmonic vibrations than the basic first harmonic-focused least squares regression, especially for forward flight.

Finally, Figure 16 shows vibration information at the third natural frequency, or 13.35 Hz, for the derived cockpit sensors and two additional sensors.

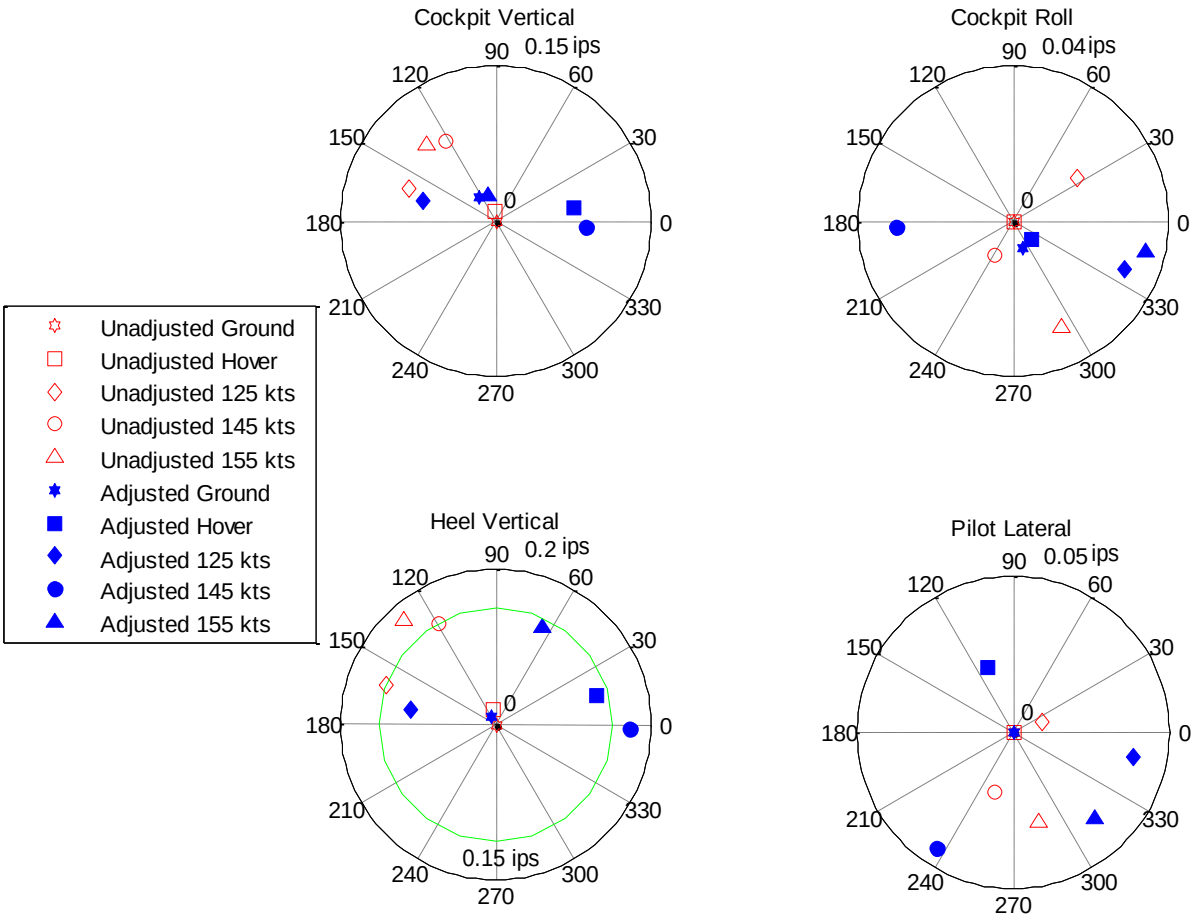

Figure 16. Third natural frequency vibration measurements from real valued genetic algorithm

In this series of flight data, only the forward flight at 145 kts in the heel vertical sensor exceeds the ideal 0.15 inches per second level after adjustments. The remaining forward flight regimes recorded by the heel vertical sensor for the third natural frequency are reduced to within the 0.15 ips range by the heuristic optimization. The genetic algorithm based RTB method does better than the 1*P* least squares regression model at maintaining low vibration levels in the cockpit roll, heel vertical, and pilot lateral sensors for the third natural frequency. As shown by an appraisal of Figure 8 versus Figure 16, the heuristic optimization RTB method performs comparably for

the vibration information collected by the cockpit vertical sensor at the third harmonic frequency. Figure 11 contrasted with Figure 16 demonstrates that the cascaded method results in comparable vibration minimization for the cockpit roll and pilot lateral sensors at frequencies of 13.35 Hz. The cascaded method outperforms the heuristic method for the cockpit vertical and heel vertical sensors at the third natural frequency. However, this is unsurprising since the last step of the cascaded method is vibration minimization in the third multiple of the rotor's natural frequency.

Table 5 demonstrates the results on $ampScore$ due to application of the genetic algorithm vibration adjustments to the original, unbalanced flight information.

Table 5. Unadjusted and adjusted vibration amplitude scores after heuristic optimization

	Unadjusted	Adjusted	Difference
$1P\ ampScore$	3.8447	1.6712	-2.1735
$2P\ ampScore$	0.6127	1.2927	0.6800
$3P\ ampScore$	0.7094	0.6766	-0.0328

Both the first and third natural frequencies of the main rotor exhibit a reduction in unwanted vibrations after the rotor track and balance genetic algorithm is applied. While the amplitude profile of the second harmonic frequency increases due to adjustment, the change is much less drastic than $2P\ ampScore$ increase from the $1P$ least squares regression method. The heuristic optimization method is also able to still maintain significant vibration reduction for the first natural frequency while also decreasing vibration in the third natural frequency.

4.6 Comparison of Algorithm Performance

All three methods of vibration minimization within the S-76C++ aircraft were implemented on 48 collections of flight data and simulated as previously described. In defining $ampScore$ to represent magnitude of undesired vibrations, a metric was developed to examine cumulative performance of each optimization technique. Comparisons can also be drawn by inspecting the series of polar plots presented throughout this chapter which show the change in vibration at varying regimes across the first natural frequency for a series of flight information. For the displayed set of flight data, the basic $1P$ minimization technique is not as effective in balancing the first and third harmonics as the cascaded minimization technique. However, this technique is better than the the cascaded harmonic technique at balancing vibrations at the second natural frequency. Balancing vibrations between multiple harmonic frequencies must incorporate improvements in as many harmonics as possible without causing significant detriment to any frequency level.

Figure 17 shows a summary of the vibration optimization methods across each of the first three harmonic frequencies of the main rotor. Each cluster of error bars represents the average and standard deviation of the amplitude of vibration across every sensor of each harmonic for all 48 test flights.

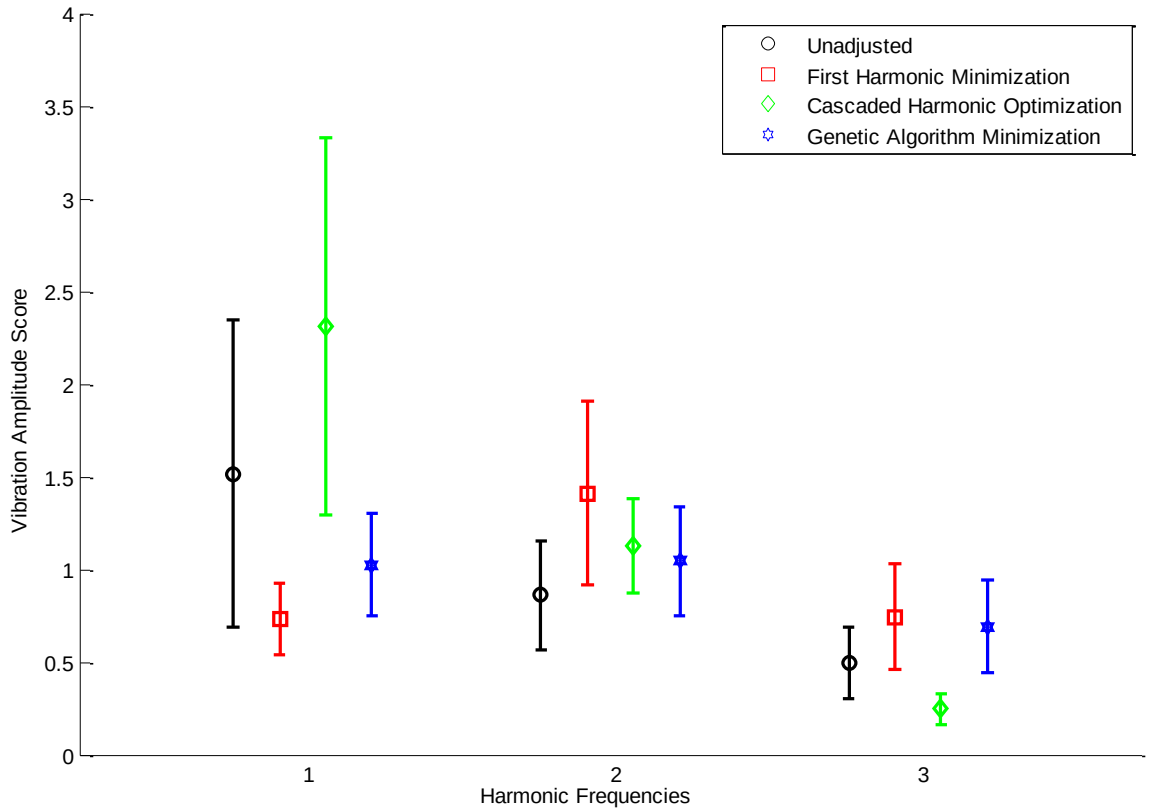

Figure 17. Vibration amplitude scores for each harmonic before adjustment, after first harmonic minimization, cascaded harmonic optimization, and integer-based real coded genetic algorithm

As seen in the previous minimization data, there are benefits and drawbacks between using each of the three RTB adjustment methods. While all three methods reduce vibration at the first natural frequency, the first harmonic minimization least squares regression performs the best at $1P$. The genetic algorithm has a lower average and smaller standard deviation for its $1P$ $ampScore$ values than the cascaded harmonic optimization for the 48 data sets. Based on the flight test data used in this study, the cascaded harmonic optimization is, on average, more likely to generate lower $2P$ $ampScore$ values than the original $1P$ method but the two methods have very similar standard deviations at the second harmonic. The genetic algorithm optimization does the best job of minimizing the average undesired vibration $ampScore$ at 8.9 Hz or $2P$ while the cascaded harmonic optimization produces the tightest deviations over the 48

flights for the $2P\ ampScore$. The cascaded harmonic optimization results in the lowest $ampScore$ for $3P$ harmonics. This can be expected since the last step of the cascaded optimization is to ensure that the $3P$ vibrations are minimized. While the first harmonic method has the largest average and spread of vibration amplitudes for the third natural frequency, the genetic algorithm has a lower average $3P$ score over the range of flight information. This is due to the ability of the genetic algorithm approach to incorporate $3P$ measurements into its analysis in ways that the first harmonic analysis does not.

CHAPTER 5

CONCLUSIONS/RESULTS

5.1 Contributions of This Thesis

This study explored a novel method of regime weighting for 4-blade rotor track and balance to emphasize importance of various flying conditions. It applied the weighting scheme to a currently proposed RTB technique, as well as to two novel methods for RTB optimization that include reduction of higher frequency harmonics. RTB adjustments were simulated with an empirically-based sensitivity model and a scoring system was established to determine optimization effectiveness. Future work in this area includes comparing performance of the proposed regime weighting scheme to established multiobjective optimization methods to determine if this proposed method produces a pareto optimal result. Additionally, significance factors can be incorporated into the different harmonic levels which will allow for varied emphasis on reduction at prescribed frequencies. Developing and validating a nonlinear model for vibrations during flight simulation will allow for more vigorous testing platform.

The cascaded harmonic minimization technique showed performance improvements on higher level harmonics as compared to the original first harmonic optimization. The integer-based real coded genetic algorithm optimization reduced $2P$ frequency vibrations at a level greater than or equal to that of the other methods. Those improvements at higher frequencies were contrasted with a decrease in performance at the first natural frequency. Though the heuristically optimized RTB method based does not always minimize the amplitude of vibratory responses for $1P$ more than the $1P$ least squares regression model, it does a superior job in vibration optimization at higher level harmonics. The genetic algorithm method also does a

more consistent job of maintaining a smaller distribution over the 48 test flights than the other approaches explored in this study.

APPENDIX A

Figure A1 shows the derivation of the least squares solution to the cost function based on Davis' minimum variance control algorithm.

$$Z_n(k+1) = Z_n(k) + T_n \cdot \theta_n$$

$$J_n = Z_n(k+1)^T \cdot W_{Zn} \cdot Z_n(k+1) + \theta_n^T \cdot W_\theta \cdot \theta_n$$

Find θ_n minimizing cost function J_n by setting $\frac{\partial J_n}{\partial \theta_n} = 0$ and solving for θ_n:

$$J_n = [Z_n(k) + T_n \cdot \theta_n]^T \cdot W_{Zn} \cdot [Z_n(k) + T_n \cdot \theta_n] + \theta_n^T \cdot W_\theta \cdot \theta_n$$

$$J_n = [Z_n(k)^T + \theta_n^T \cdot T_n^T] \cdot W_{Zn} \cdot [Z_n(k) + T_n \cdot \theta_n] + \theta_n^T \cdot W_\theta \cdot \theta_n$$

$$J_n = Z_n(k)^T \cdot W_{Zn} \cdot Z_n(k) + Z_n(k)^T \cdot W_{Zn} \cdot T_n \cdot \theta_n + \theta_n^T \cdot T_n^T \cdot W_{Zn} \cdot Z_n(k)$$
$$+\theta_n^T \cdot T_n^T \cdot W_{Zn} \cdot T_n \cdot \theta_n + \theta_n^T \cdot W_\theta \cdot \theta_n$$

$$\frac{\partial J_n}{\partial \theta_n} = [Z_n(k)^T \cdot W_{Zn} \cdot T_n]^T + [T_n^T \cdot W_{Zn} \cdot Z_n(k)] + [T_n^T \cdot W_{Zn} \cdot T_n] \cdot \theta_n$$
$$+[T_n^T \cdot W_{Zn} \cdot T_n]^T \cdot \theta_n + W_\theta \cdot \theta_n + W_\theta^T \cdot \theta_n = 0$$

$$\frac{\partial J_n}{\partial \theta_n} = [T_n^T \cdot W_{Zn} \cdot Z_n(k)] + [T_n^T \cdot W_{Zn} \cdot Z_n(k)] + [T_n^T \cdot W_{Zn} \cdot T_n] \cdot \theta_n$$
$$+[T_n^T \cdot W_{Zn} \cdot T_n] \cdot \theta_n + W_\theta \cdot \theta_n + W_\theta \cdot \theta_n = 0$$

$$\frac{1}{2}\{2 \cdot [T_n^T \cdot W_{Zn} \cdot Z_n(k)] + 2 \cdot [T_n^T \cdot W_{Zn} \cdot T_n] \cdot \theta_n + 2 \cdot [W_\theta \cdot \theta_n]\} = \frac{1}{2}[0]$$

$$[T_n^T \cdot W_{Zn} \cdot Z_n(k)] + [T_n^T \cdot W_{Zn} \cdot T_n + W_\theta] \cdot \theta_n = 0$$

$$[T_n^T \cdot W_{Zn} \cdot T_n + W_\theta] \cdot \theta_n = -[T_n^T \cdot W_{Zn} \cdot Z_n(k)]$$

$$\theta_n = -[T_n^T W_{Zn} T_n + W_\theta]^{-1} \cdot [T_n^T W_{Zn} Z_n(k)]$$

Figure A1. Least squares regression solution proof

REFERENCES

[1] M. Robinson, "Helicopter Track and Balance Theory," *Aircraft Maintenance Technology*, 1999.

[2] A. Rosen and R. Ben-Ari, "Mathematical Modelling of a Helicopter Rotor Track and Balance: Theory," *Journal of Sound and Vibration*, pp. 589-603, 1997.

[3] M. Renzi, "Air Force Institute of Technology Thesis," Jun. 2004.

[4] L. Johnson. History: Helicopter Rotor Smoothing. [Online]. http://www.dssmicro.com/theory/dsrothst.htm

[5] V. Giurgiutiu, G. Craciun, and A. Rekers, "Cost Benefit Analysis Models for Evaluation of a VMEP/HUMS Project," in *55th Meeting of the Society for Machinery Failure Prevention Technology*, Virginia Beach, 2001.

[6] E. Bechhoefer, A. Fang, and D. Van Ness, "An Expert System for Rotor Track and Balance," in *AHS/AIAA Airworthiness, CBM, and HUMS Specialists' Meeting*, Huntsville, 2011.

[7] S. Bhadra and R. Ganguli, "Aeroelastic Optimization of a Helicopter Rotor Using Orthogonal Array-Based Metamodels," *American Institute of Aeronautics and Astronautics*, pp. 1941-1951, 2006.

[8] S. Murugan, R. Ganguli, and D. Harursampath, "Robust Aeroelastic Optimization of Composite Helicopter Rotor," in *International Conference of Engineering Optimization*, Rio de Janeiro, 2008.

[9] N. Roy and R. Ganguli, "Helicopter rotor blade frequency evolution with damage growth

and signal processing," *Journal of Sound and Vibration*, pp. 821-851, 2005.

[10] P. Pawar and R. Ganguli, "Helicopter Rotor Health Monitoring - A Review," *Journal of Aerospace Engineering*, pp. 631-647, 2007.

[11] E. Bechhoefer, A. Fang, and D. Van Ness, "Improved Rotor Track and Balance Performance," 2010.

[12] H. Taitel, K. Danai, and D. Gauthier, "Helicopter Track and Balance with Artificial Neural Nets," *Journal of Dynamic Systems, Measurement, and Control* , vol. 117, no. 2, pp. 226-275, 1995.

[13] R. Ben-Ari and A. Rosen, "Mathematical Modelling of a Helicopter Rotor Track and Balance: Results," *Journal of Sound and Vibration*, pp. 605-620, 1997.

[14] C. Theodore and R. Celi, "Helicopter Flight Dynamic Simulation with Refined Aerodynamics and Flexible Blade Modeling," in *56th Annual Forum of the American Helicopter Society*, Virginia Beach, 2000.

[15] S. Wang, K. Danai, and W. Mark, "A probability-based approach to helicopter rotor tuning," *Journal of the American Helicopter Society*, vol. 50, no. 1, pp. 56-64, 2005.

[16] D. Yang, S. Wang, and K. Danai, "Helicopter Track and Balance by Interval Modeling," in *American Helicopter Society 57th Annual Fourm*, Washington DC, 2001.

[17] E. Bechhoefer and D. Power, "IMD HUMS Rotor Track and Balance Techniques," in , 2003.

[18] D. Fusato and R. Celi, "Multidisciplinary Design Optimization for Aeromechanics and Handling Qualities," in *European Rotorcraft Fourm*, Bristol, UK, 2002.

[19] Bradley, Hax, and Magnanti, *Applied Mathematical Programming*. Addison-Wesley, 1977.

[20] T. van Engelen, "Design Model and Load Reduction Assessment for Multi-Rotational Mode Individual Pitch Control (Higher Harmonics Control)," in *European Wind Energy Conference*, Athens, 2006.

[21] R. Cheng and R. Celi, "Optimum 2/Rev Inputs for Improved Rotor Performance," in *Northeast Region Active Controls Technology Conference of the American Helicopter Society*, Fairfield County, 2000.

[22] R. Cheng, C. Theodore, and R. Celi, "Effects of Higher Harmonic Control on Rotor Performance," in *56th Annual Forum of the American Helicopter Society*, Virginia Beach, 2000.

[23] M. Lovera and P. Colaneri, "Discrete-Time, Closed-Loop Aeromechanical Stability Analysis of Helicopters with Higher Harmonic Control," *Journal of Guidance, Control, and Dynamics*, pp. 1249-1260, 2006.

[24] R. Ganguli, I. Chopra, and D. Haas, "Helicopter Rotor System Fault Detection Using Physics-Based Model and Neural Networks," *AIAA Journal*, vol. 36, no. 6, pp. 1078-1086, 1998.

[25] D. E. Goldberg, *Genetic Algorithms in Search, Optimization and Machine Learning*. Addison-Wesley, 1988.

[26] Z.-Q. Chen and R.-L. Wang, "An Efficient Real-coded Genetic Algorithm for Real-Parameter Optimization," in *Sixth International Conference on Natural Computation*, Yantai, 2010.

[27] T. Hamernik, E. Garcia, and D. Stech, "Optimal Placement of Damped Struts Using Simulated Annealing," *Journal of Spacecraft and Rockets*, vol. 32, no. 4, pp. 653-661, 1995.

[28] S. M. Sait and H. Youssef, *Iterative Computer Algorithms with Applications in Engineering*. Los Alamitos: IEEE Computer Society, 2000.

[29] P. Reed, B. Minsker, and D. Goldberg, "Designing a competent simple genetic algorithm for search and optimization," *Water Resources Research*, vol. 36, no. 12, pp. 3757-3761, 2000.